Article:
Bryant, Dan, Elzein, Atallah El Zein, Newland, Mike et al. (9 more authors) (2021) Importance of Oxidants and Temperature in the Formation of Biogenic Organosulfates and Nitrooxy Organosulfates. ACS Earth and Space Chemistry. ISSN 2472-3452

https://doi.org/10.1021/acsearthspacechem.1c00204

ACS EARTH AND SPACE CHEMISTRY

http://pubs.acs.org/journal/aesccq

Article

Importance of Oxidants and Temperature in the Formation of Biogenic Organosulfates and Nitrooxy Organosulfates

Daniel J. Bryant,* Atallah Elzein, Mike Newland, Erin White, Stefan Swift, Amy Watkins, Wei Deng, Wei Song, Sainan Wang, Yanli Zhang, Xinming Wang, Andrew R. Rickard, and Jacqueline F. Hamilton

Cite This: https://doi.org/10.1021/acsearthspacechem.1c00204

Read Online

ACCESS | Metrics & More | Article Recommendations | Supporting Information

ABSTRACT: Biogenic secondary organic aerosol (BSOA) makes up a significant proportion of organic aerosol, and its formation chemistry, composition, and physical properties can be influenced by anthropogenic emissions, especially in urban areas. Organosulfates (OSs) are an important class of tracers for BSOA and have been well-studied over the past decade, although detailed ambient studies of diurnal variations are still lacking. In this study, fine particulate matter samples were collected eight times a day across summer and winter campaigns at an urban site in Guangzhou, China. Guangzhou is heavily influenced by both biogenic and anthropogenic emissions, allowing for biogenic−anthropogenic interactions to be studied. Individual OSs and nitrooxy OSs (NOSs) species derived from monoterpenes and isoprene were analyzed using ultrahigh-performance liquid chromatography tandem mass spectrometry (UHPLC−MS^2) and quantified using three authentic and proxy standards. The observations show strong diurnal variations of monoterpene derived OSs and NOSs, which peaked during the night, with concentrations increasing from the early evening, highlighting the role of NO_3-oxidation chemistry. Isoprene derived OSs/NOSs showed strong seasonal profiles, with summer and winter average concentrations of 181.8 and 69.5 ng m^{-3}, respectively, with exponential increases observed at temperatures above 30 °C. Low-NO formation pathways were dominant in the summer, while high-NO pathways became more important in the winter. Isoprene OS formation was strongly dependent on the availability of particulate sulfate (SO_4^{2-}), suggesting an extensive heterogeneous chemistry of oxidized isoprene species. Overall, this study provides further insights into biogenically derived OS and NOS formation within highly anthropogenically influenced environments.

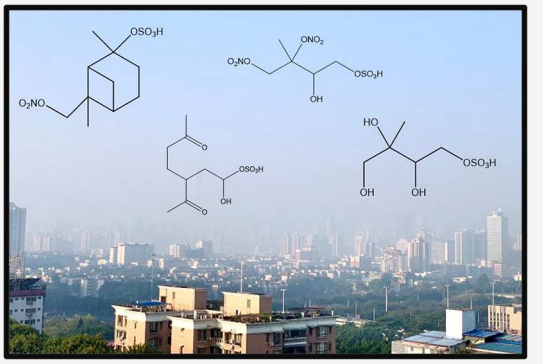

KEYWORDS: *isoprene, monoterpenes, heterogeneous, diurnal variations, sulfate, Orbitrap*

INTRODUCTION

Organosulfates (OSs) are key contributors of atmospheric secondary organic aerosol and have been detected in ambient aerosols in both clean and polluted sites around the world.[1−10] OSs have been shown to make up significant portions of organic aerosol (OA) and $PM_{2.5}$ (particulate matter less than 2.5 μm in diameter) mass,[11−13] with isoprene derived OSs accounting for up to 8% of organic matter.[14] Radiocarbon measurements have shown that OA is dominated by modern carbon even in urban areas,[15−19] suggesting that biogenic sources could be playing a key role in OA and $PM_{2.5}$ formation.

Chamber studies have shown the formation of particle-bound OSs from gas-phase oxidation of biogenic volatile organic compounds (VOCs) such as isoprene,[20−22] monoterpenes,[7,21] sesquiterpenes,[23] and green leaf volatiles[24] via OH, NO_3, and O_3 oxidation pathways in the presence of sulfate aerosol or SO_2. Many of the species identified in these chamber studies have also been detected in ambient samples, with isoprene derived OSs as some of the most abundant biogenic OS markers quantified.[4,25] It should be noted that while these OS and NOS species are termed as BSOA due to their VOC precursors they are formed through interactions with anthropogenic pollutants. The formation mechanisms of OSs have been studied extensively,[13] with OS formation through an acid catalyzed ring opening of epoxides considered to be the most important route,[7,21,26−28] especially for those derived from isoprene. However, several other routes have been proposed such as sulfate radical addition to an unsaturated precursor in the aqueous phase,[29,30] direct sulfate esterification of an alcohol precursor,[21] or the replacement of nitrate groups within organonitrate species with sulfate.[31,32] Recent studies have reported the formation of OSs both directly and indirectly from the reaction of unsaturated species

Special Issue: Mario Molina Memorial

Received: June 20, 2021
Revised: August 24, 2021
Accepted: August 24, 2021

with SO_2.[33−35] Nitrooxy-OSs (NOSs) are a sub class of OS and have been observed in several locations,[1,6,8,36−43] but their formation pathways are less well-studied.[21,44−46] NOS species have been shown to form from the reaction of sulfate with organic nitrate species, formed during OH photo-oxidation of VOCs via a reaction of the peroxy radicals with NO. Organic nitrates can also be formed from nitrate radical initiated oxidation of VOCs,[45,47] which becomes increasingly important at night when the concentration of NO_3 radicals is higher and concentrations of OH are reduced.[48] Recent studies by Liebmann et al. in 2019 and Hamilton et al. in 2021 indicate that, under low-NO conditions, nitrate radical chemistry can also play an important role in organic nitrate production during the daytime.[48,49]

Several factors make the accurate identification and quantification of individual OS species in ambient aerosol challenging,[50] but it is important for understanding aerosol formation, properties, and the factors that affect the OS contribution to $PM_{2.5}$. First, the compositionally complex samples, which contain thousands of multifunctional compounds, can lead to significant matrix effects as seen for isoprene derived OSs (OSi) species.[1,6] Second, BSOA suffers from a lack of authentic standards, meaning proxy standards must be used. Recently, several studies have synthesized a number of OS authentic standards derived from isoprene and monoterpenes and quantified them in ambient samples.[10,51,52] These studies have shown that differences in ionization efficiencies between several authentic monoterpene OSs and proxy standards can be significant, with Wang et al. in 2017 showing a factor 6.4 difference between the two extremes on the ionization scale, highlighting the need for future studies to focus on more accurate quantification.[51]

Guangzhou is a megacity in South China situated in the Pearl River Delta (PRD) region, with an approximate population of 15 million. To the south are the densely populated cities of Macao, Shenzen, and Hong Kong, while there is relatively less urbanization to the north of Guangzhou. Guangzhou like the rest of China historically experiences high levels of pollution but less extremely than northern cities. Recently introduced pollution controls have started to take effect, reducing the concentrations of some pollutants.[53,54] Unlike in some other cities in China, nonfossil secondary species account for higher fractions of OA during both high- and low-PM episodes in Guangzhou even during the winter.[12] Guangzhou has a subtropical climate, with mild winters and hot rainy summers due to Asian monsoons. This promotes high emissions of biogenic VOCs[55] into a region that is heavily influenced by anthropogenic emissions, providing a good case study of biogenic−anthropogenic interactions.

Multiple studies have now identified and quantified OSs in ambient samples, however many of these used long sampling times,[4,6,8,10] which does not allow for ambient diurnal variations to be resolved, thus hindering the determination of formation mechanisms and sources. This study employs one of the highest time resolution filter collection regimes for OS and NOS to date, with eight filters collected per day in Guangzhou. Over 300 ambient $PM_{2.5}$ samples were collected over two intensive campaigns during the summer and winter and were analyzed using ultrahigh-performance liquid chromatography tandem mass spectrometry (UHPLC−MS^2). Over 40 biogenic OS and NOS species were quantified using a mixture of authentic and proxy standards. Diurnal variations of different tracers were comprehensively investigated and linked to different formation pathways. Biogenic−anthropogenic interactions were also investigated to better assess the formation pathways of OSs and NOSs under real atmospheric conditions.

MATERIALS AND METHODS

Filter Collection. Ambient aerosol filter samples were collected in Guangzhou, China at the Guangzhou Institute for Geochemistry (GIG) as part of the Natural Environmental Research Council's (NERC) NITRO-PM project. The sampling took place on top of a 12-story mixed use office and laboratory building (23.145 N, 113.364 E). The site was surrounded by residential buildings, with a six-lane road ∼500 m to the south and a forest park ∼4 km to the north. $PM_{2.5}$ samples were collected during the summer (31/07/2019−23/08/2019, n = 147) and winter (20/11/2019−12/12/2019, n = 167) using an Ecotech HiVol (Ecotech, Knoxfield, Australia) with a selective $PM_{2.5}$ inlet and a flow rate of 1.1 m^3 min^{-1}. Filters were prebaked to remove residual organics at 500 °C for 5 h before use. After collection, samples were wrapped in foil and stored at −20 °C until analysis. Filter samples were collected eight times a day on most days: 06:00−08:00, 08:00−10:00, 10:00−13:00, 13:00−15:00, 15:00−17:00, 17:00−19:00, 19:00−21:00, 21:00−06:00. On some days, lower time resolution samples were collected due to extreme weather conditions, including Tropical Cyclone Wipha between the first and third of August 2019.

Extraction. The extraction of the filter is similar to that used previously by Bryant et al. in 2020. Initially, using a standard square filter cutter, an aliquot of the filter was taken, with an area of 47.61 cm^2 (6.9 cm × 6.9 cm), which was then cut into roughly 1 cm^2 pieces and stored in a 20 mL glass vial. Next, 8 mL of LC−MS grade MeOH (Optima, Fisher Chemical) was added to the sample and sonicated for 45 min. Ice packs were used to keep the bath temperature below room temperature, with the water swapped midway through. Using a 5 mL plastic syringe, the MeOH extract was then pushed through a 0.22 μm filter (Millipore) into another sample vial. An additional 2 mL (2 × 1 mL) of MeOH was added to the filter sample and then extracted through the filter to give a combined extract of ∼10 mL. This extract was then reduced to dryness using a Genevac vacuum concentrator. The dry sample was then reconstituted in 50:50 MeOH/H_2O (Optima, Fisher Chemical) for analysis. Extraction efficiencies of 2-methyl glyceric acid organosulfate, camphorsulfonic acid, and pinonic acid were determined using authentic standards spiked onto a prebaked clean filter and recoveries were calculated to be 71%, 99%, and 85%, respectively.

Ultrahigh-Performance Liquid Chromatography Tandem Mass Spectrometry (UHPLC−MS^2). The extracted fractions of the filter samples were analyzed using an Ultimate 3000 UHPLC (Thermo Scientific) coupled to a Q Exactive Orbitrap MS (Thermo Fisher Scientific) using data dependent tandem mass spectrometry (ddMS^2) with a heated electrospray ionization source (HESI). The UHPLC method uses a reversed-phase 5 μm, 4.6 mm × 100 mm, polar end-capped Accucore column (Thermo Scientific, 17326-102130) held at 40 °C. The mobile phase consisted of water (A) and methanol (B), both with 0.1% (v/v) of formic acid (98% purity, Acros Organics). A gradient elution was used, starting at 90% (A) with a 1 min postinjection hold, decreasing to 10% (A) at 26 min, returning to the starting mobile-phase conditions at 28 min, followed by a 2 min hold, allowing the re-equilibration of the column. The flow rate was set to 0.3 mL min^{-1}. A sample

https://doi.org/10.1021/acsearthspacechem.1c00204
ACS Earth Space Chem. XXXX, XXX, XXX−XXX

injection volume of 4 μL was used. The capillary and auxiliary gas heater temperatures were set to 320 °C, with a sheath gas flow rate of 45 (arb.) and an auxiliary gas flow rate of 20 (arb.). Spectra were acquired in the negative ionization mode with a scan range of mass-to-charge (m/z) 50−750. Tandem mass spectrometry was performed using higher-energy collision dissociation with a stepped normalized collision energy of 65 115. The isolation window was set to m/z 2.0 with a loop count of 10, selecting the 10 most abundant species for fragmentation in each scan.

Data Processing and Compound Library. A mass spectral library was built using the compound database function in Tracefinder 4.1 General Quan software (Thermo Fisher Scientific). To build the library, compounds from previous studies[23,30,47,56−58] were searched for in an afternoon and a nighttime filter sample extract analysis using the Xcalibur software. Identified compounds were input into the compound library in the generic form: $C_cH_hO_oN_nS_s$ (where c, h, o, n, and s represent the number of carbon, hydrogen, oxygen, nitrogen, and sulfur atoms, respectively). Where multiple isomers were observed, each isomer was added to the library independently, on the basis of its retention time (RT). The UHPLC/ESI-HR-MS data for each standard and ambient sample were analyzed using Tracefinder general Quan software (Thermo Fisher Scientific). Blank subtractions were undertaken for all ambient samples, using a field blank. Tracefinder extracted compound peak areas from each sample on the basis of the assigned library. The mass tolerance of the method was set to 3 ppm, with the RT window set to 10 s. The peak tailing factor was set to 2.0 and the detection algorithm used was ICIS, with a nearest RT detection strategy. The minimum signal-to-noise (S/N) for a positive identification was set to 3.0. The suitability of the peak was also assessed for a positive identification, with the peak height at which to compare the symmetry of the left and right sides of the peaks set to 40% and symmetry threshold, which is the minimum percentage difference considered symmetrical set to 70%.

Calibration and Matrix Effects. The accurate quantification of BSOA is difficult owing to a lack of authentic standards. This study employs one proxy (camphorsulfonic acid, Sigma-Aldrich) and two authentic standards (2-methyl tetrol organosulfate (2-MT-OS) and 2-methyl glyceric acid organosulfate (2-MG-OS)). The authentic standards were obtained from Surratt's group at The University of North Carolina at Chapel Hill.[59] Standards were run across a 9-point calibration curve (2 ppm−7.8 ppb, $R^2 > 0.99$). We also evaluated the matrix effect of the ambient samples on the signal response of the three standards used for quantification. The measured signal intensity of the standards in a blank solvent matrix were compared to the ambient aerosol matrix. A 10 μL mixture containing camphorsulfonic acid, 2-MG-OS, and 2-MT-OS at 10 ppm was spiked into either 100 μL of ambient filter sample extract or into 100 μL of blank 50:50 (MeOH/H_2O) solvent. The samples were run as described above. The matrix effect factors were then calculated by taking the compound areas from the spiked ambient samples, subtracting the areas of compounds that were already present in the ambient sample, and then dividing by the compound areas in the blank matrix. If no matrix effect was present, the ratio would equal 1. Table S1 shows the ratios across eight ambient samples collected during both campaigns, which represent a mixture of high and low $PM_{2.5}$ concentrations across different times of day. 2-MT-OS showed a significant matrix effect, with an average matrix ratio of 0.29 ± 0.23, suggesting a 71% suppression in signal response. In contrast, 2-MG-OS showed little matrix suppression with an average of 0.84 ± 0.18. Matrix correction factors were applied alongside calibrations to different compound classes and for compounds eluting at different times. Species eluting before 2 min (mainly isoprene-derived OS) were quantified using an average gradient of 2-MG-OS and 2-MT-OS across the 9-point calibration curve, and a matrix correction factor of 0.57 ± 0.16 was applied on the basis of the average matrix effect factors for 2-MG-OS and 2-MT-OS. 2-MG-OS and 2-MT-OS identified in the ambient samples were quantified using their own authentic standards and corrected with their own specific factors of 0.84 ± 0.18 and 0.29 ± 0.14, respectively. For species eluting after 2 min, camphorsulfonic acid was used a proxy and corrected with a matrix effect factor of 0.68 ± 0.23. Camphorsulfonic acid has been shown to be the most accurate proxy standard by comparison with synthesized authentic monoterpene OS standards from α-/β-pinene and limonene.[51] Due to the limited number of studies investigating the matrix effects of aerosol samples, conclusions of the underlying causes cannot be drawn. However, the suppression is likely due to the large numbers of coeluting inorganic and organic species, reducing the ionization efficiency of the marker compounds.[60]

Uncertainties for the calibration of 2-MG-OS and 2-MT-OS were calculated from the standard deviation uncertainty in the repeated measurements of the nine calibration points and the standard deviation of the matrix effects calculated in Table S1. The uncertainties associated with 2-MG-OS and 2-MT-OS were calculated to be 25% and 48%, respectively, mainly due to the large uncertainties in the matrix correction factors. For species quantified by the average of 2-MG-OS and 2-MT-OS, we estimated the error to be the sum of the errors associated with 2-MG-OS and 2-MT-OS (56%). For OS/NOS species eluting after 2 min, the uncertainty (36.5%) was estimated on the basis of the standard deviation of the camphorsulfonic acid calibration and the difference in matrix effect factors as well as the use of proxy standards. Recently, a study that synthesized authentic NOS_{MT} standards quantified the same NOS_{MT} species as in this study and observed very similar concentrations.[61] For example, for the MW295 isomers, they found a mean concentration of 12.3 ng m^{-3} in Guangzhou in the winter, with the full range of observed concentrations across four cities (Hong Kong, Guangzhou, Beijing, and Shanghai) of 1.2−39.3 ng m^{-3}. This compares very well with our estimated mean concentration of 11.1 ng m^{-3} and range of 0.32−26.7 ng m^{-3}.[61] This would suggest that the use of the camphorsulfonic acid proxy standard gives a reasonable calibration compared to the use of authentic standards.

Gas-Phase Measurements. Additional gas-phase and meteorological measurements were collected alongside the filter samples at the site (Table S2). Data included the following nitrogen species: NO, NO_2, and NO_X measured by Chemiluminescence with a Thermo Scientific 42i-TL. Ozone was measured via ultraviolet with a Thermo Scientific 49i, and SO_2 was measured via pulsed fluorescence with a Thermo Scientific 43i-TLE. Finally, $PM_{2.5}$ was measured by a continuous particulate monitor (BAM-1020, Met One instruments Inc.).

Ion Chromatography. Inorganic sulfate and nitrate were quantified using ion chromatography using a method outlined in Xu et al. in 2020.[62] An area of 6.9 cm^2 was cut from each filter and cut into small pieces and transferred to a 15 mL vial.

https://doi.org/10.1021/acsearthspacechem.1c00204
ACS Earth Space Chem. XXXX, XXX, XXX−XXX

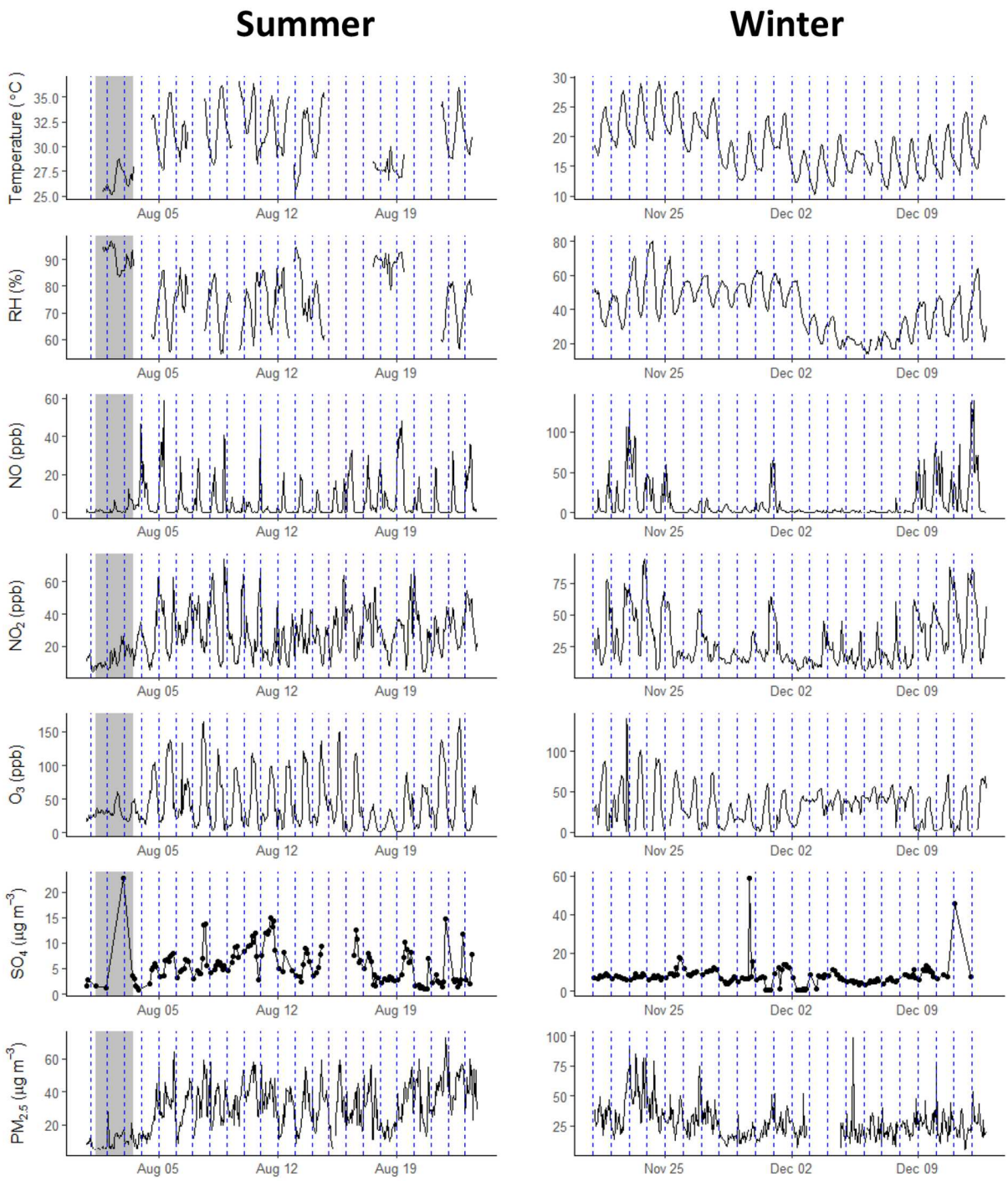

Figure 1. Time series of pollutants across the summer (left) and winter (right) campaigns. The highlighted section in the summer campaign indicates typhoon Wipha. The blue dotted lines indicate midnight of each day.

Two milliliters of 18.2 MΩ·cm deionized water was added to each vial before being sonicated for 30 min. A Dionex ICS-1100 with a DS6 heated conductivity cell and a Dionex AS-DV carousel with Chromeleon Data system software were used for data analysis. For anion mode, a Dionex AG14A 4 mm guard column was used with a Dionex AS14A 4 mm analytical column and a DRS Dionex ADRS 600 suppressor. The anion eluent was prepared using 1.698 g of Na_2CO_3 and 0.168 g of $NaHCO_3$ with 2 L of >18.2 MΩ deionized water added 1 L at a time. After each 1 L addition, the eluent bottle was sonicated in degas mode for 30 min. The column was equilibrated at an oven temperature of 35 °C and a current of 45 mA. Anions were calibrated using 12-point calibration curves: 0.01, 0.05, 0.1, 0.25, 0.5, 1, 2.5, 5, 10, 25, 50, and 100 ppm. The autosampler delivered 350 μL at 4 mL/min to the instrument that used 100 μL and was at a flow rate of 1 mL/min for ion separation and detection.

RESULTS AND DISCUSSION

Meteorology and Anthropogenic Pollutants. Figure 1 shows the time series of the following measured pollutants: NO, NO_2, O_3, and $PM_{2.5}$ alongside particulate sulfate during

https://doi.org/10.1021/acsearthspacechem.1c00204
ACS Earth Space Chem. XXXX, XXX, XXX−XXX

the two sampling periods (summer on the left, winter on the right). Mean and maximum values are shown in Table S2 for both campaigns, along with additional aerosol anion data. The meteorological conditions between the two campaigns were quite different with a mean temperature (±sd) of 30.4 ± 2.9 °C in the summer compared to 18.3 ± 4.2 °C during the winter campaign. The mean relative humidity in summer (77.6 ± 10.6%) was roughly double that of the winter campaign (40.6 ± 14.7%). The mean wind speed was much lower during the winter campaign (1.9 ± 1.0 ms^{-1}) compared to that of the summer (6.0 ± 3.9 ms^{-1}).

Figure S1 shows the average diurnal profiles for temperature, RH, O_3, NO, NO_2, SO_2, and $PM_{2.5}$. The mean ozone mixing ratios were higher in the summer (43.1 ± 37.3 ppbv) than the winter (31.8 ± 23.1 ppbv) with a strong diurnal variation peaking midafternoon. The mean NO concentration was around double in the winter campaign (12.1 ± 22.6 ppbv) compared to that of the summer (5.4 ± 9.4 ppbv). NO mixing ratios showed a strong diurnal variation in both campaigns, peaking during the morning rush hour. Due to ozone titration, NO concentrations reached <0.5 ppb on average in the afternoon during the summer campaign similar to previous observations in Beijing.[63] NO was also lower during the day in winter with an afternoon average of ∼1.5 ppb. During the winter, several periods of high NO concentrations were observed, as shown in Figure 1 (20−25 November, 30 November, and 9−12 December). The SO_2 mixing ratios were only measured in the winter campaign with an average of 2.9 ± 1.1 ppbv, with a morning peak around 07:00−08:00 am (Figure S2). Inorganic ions were measured via ion chromatography. Lower mean particulate SO_4^{2-} concentrations were observed in the summer (5.6 ± 3.7 $\mu g\ m^{-3}$) compared to those in winter (7.8 ± 6.0 μgm^{-3}), while the average particulate NO_3^- concentration during the winter campaign (6.0 ± 6.0 $\mu g\ m^{-3}$) was double that of the summer campaign (3.6 ± 3.0 $\mu g\ m^{-3}$). The mean $PM_{2.5}$ concentrations were similar across both campaigns, with neither campaign showing a strong diurnal variation.

Biogenic Organosulfates and Nitrooxyorganosulfates. *Monoterpene Nitrooxy Organosulfates (NOS_{MT}).* The monoterpene derived NOS (NOS_{MT}) species include 26 $C_{9/10}$ species with five unique molecular formulas across both campaigns ($C_{10}H_{17}NO_7S$, $C_{10}H_{17}NO_8S$, $C_{10}H_{17}NO_9S$, $C_{10}H_{19}NO_9S$, and $C_9H_{15}NO_8S$). Species matching these formula have been shown to form in laboratory simulations from monoterpene photo-oxidation in the presence of NO and from dark NO_3 radical chemistry.[56] In this study, the total NOS_{MT} mean (±sd) concentration in the summer was 8.3 ± 8 ng m^{-3} and that in winter was 13.1 ± 7.1 ng m^{-3}. The increase during the winter campaign may be due to higher NO_X concentrations, higher sulfate levels, or lower temperatures promoting condensation.[64] Higher summertime biogenic monoterpene concentrations have been modeled previously in the PRD.[65] Potential additional, nonbiogenic sources of gas-phase emissions of monoterpenes in the winter include increased biomass burning or cooking.[66−72] However, the lack of gas-phase observations of monoterpenes means it is not possible to draw conclusions currently. $C_{10}H_{17}NO_7S$ was the dominant species across both campaigns, contributing ∼85% of the NOS_{MT} mass on average, with summer and winter concentrations of 7.1 ± 7.3 and 11.1 ± 6.5 ng m^{-3}, respectively. These concentrations are comparable to concentrations observed in Shanghai (summer average, −5.71 ng m^{-3}; winter average, −4.22 ng m^{-3})[6] and summertime in Beijing (12 ng m^{-3})[73] with $C_{10}H_{17}NO_7S$ again identified as the most dominant NOS_{MT} across both studies. These concentrations are also similar to those quantified by authentic standards across four Chinese megacities (Hong Kong, 5.61 ng m^{-3}; Guangzhou, 12.32 ng m^{-3}; Shanghai, 16.51 ng m^{-3}; Beijing, 13.15 ng m^{-3}). He et al. in 2014 also observed higher wintertime NOS_{MT} concentrations at a regional background site in the PRD, although the reported $C_{10}H_{17}NO_7S$ concentrations were much higher (52.4 and 151 ng m^{-3} for summer and winter, respectively).[74]

Parts a and b of Figure 2 show the mean concentration of the sum of NOS_{MT} species during each filter collection time

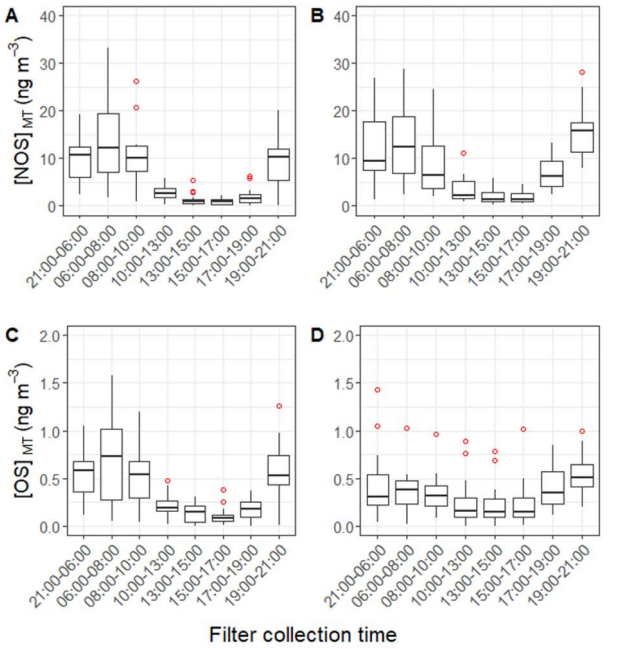

Figure 2. Diurnal variations of (A) NOS_{MT} during summer, (B) NOS_{MT} during winter, (C) OS_{MT} during summer, and (D) OS_{MT} during winter. The lower and upper parts of the box represent the 25th and 75th percentiles, with the upper and lower lines extending no further than 1.5× the interquartile range of the highest and lowest values within the line, respectively. Any data points outside of this range are shown as red circles.

across the summer and winter campaigns, respectively. Several of the tracers were only identified in a small number of samples, and only tracers identified in more than 40% of the samples were included in the diurnal variations and carried forward for correlations. A strong diurnal variation is seen during both campaigns, peaking at night, with a minimum during the afternoon. A more pronounced increase in concentrations is observed in the 17:00−19:00 filter during the winter compared to that in the summer, likely due to the earlier sunset of 17:45 compared to 19:00 in the temperatures associated with lower tracer concentrations in the summer. This nighttime enhancement was also seen previously in Beijing and Shanghai.[6,73] Although monoterpenes were not measured as part of this study, nighttime enhancements of monoterpenes have been observed previously in Beijing.[73] In contrast, He et al. in 2014 observed that $C_{10}H_{17}NO_7S$ in the background PRD peaked during the day, with daytime concentrations on average ∼3 times higher than those at night.

https://doi.org/10.1021/acsearthspacechem.1c00204
ACS Earth Space Chem. XXXX, XXX, XXX−XXX

Surratt et al. in 2008 outlined both a daytime and nighttime route to the formation of the dominant NOS_{MT} ($C_{10}H_{17}NO_7S$).[21] The nighttime formation pathway proceeds via NO_3 radical oxidation, while the daytime formation route predominantly proceeds via hydroxyl radical oxidation followed by a reaction of the peroxy radical with NO. NOS_{MT} can also be formed during the day and night through monoterpene ozonolysis.[75] NOS_{MT} concentrations increased strongly with increasing SO_4^{2-} concentrations in summer nighttimes (Figure S3), but limited correlations were observed during the day and in the winter. This suggests that, during the summer, nighttime SO_4^{2-} is a limiting reagent, but other periods are VOC oxidation limited. The maximum observed NOS_{MT} concentrations during the summer and winter were 58.7 and 28.3 ng m^{-3}, respectively, both of which were observed during the 06:00−08:00 filter collection. The diurnal variation of monoterpenes measured in a previous study indicates higher monoterpene concentrations at night in Guangzhou, while daytime concentrations were roughly half the nighttime concentrations.[76] As such, the lower daytime NOS_{MT} concentrations could be linked to the monoterpene emission profile, decomposition via photolysis, or further OH oxidation of the NOS species..[77,78] NOS_{MT} concentrations showed generally decreased concentrations with increasing temperatures throughout the day across both campaigns (Figure 3), although the trend is not strong. Under higher temperatures, increased photolysis is expected, leading to higher OH radical concentrations[79] as well as photolysis of NOS_{MT} species. Therefore, under higher temperatures during the day, an enhanced degradation of the NOS_{MT} markers is expected. Under higher temperatures, NOS_{MT} species will be more volatile and thus their equilibrium partitioning may shift toward the gas phase. In contrast, at night, higher temperatures lead to increased NOS_{MT} concentrations, potentially as a result of higher monoterpene emissions.[80]

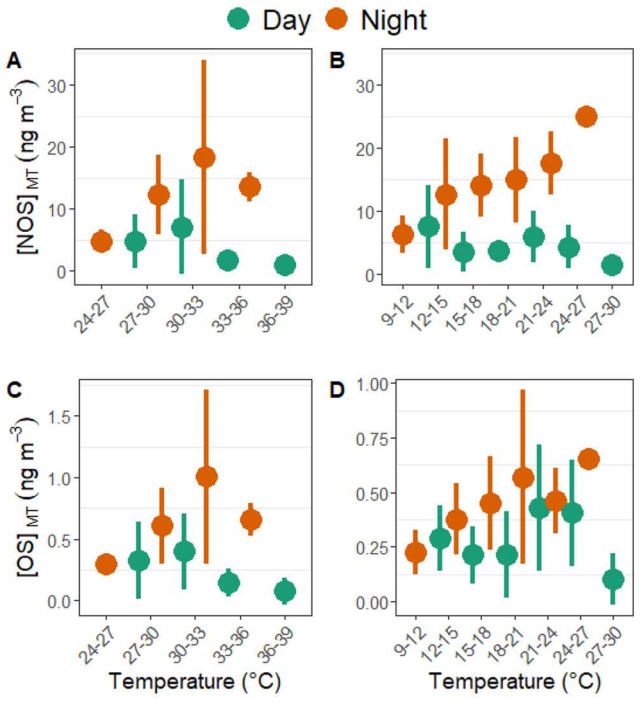

Figure 3. Binned correlation plots between markers and temperature: (A) NOS_{MT} during summer, (B) NOS_{MT} during winter, (C) OS_{MT} during summer, and (D) OS_{MT} during winter. The points represent the mean concentration ± SD within each temperature range bin.

No conclusive direct correlation between NOS_{MT} concentrations and NO_2 was observed across either campaign, with R^2 < 0.10 both during the day and at night, although higher NOS_{MT} concentrations were generally observed with elevated NO_2 levels in both seasons within reasonable uncertainties, suggesting that formation via NO_3 initiated oxidation is important (Figure S4).

On the basis of previous observations in Beijing, NO_3 initiated oxidation can happen both at night and also during the day as a result of very low NO mixing ratios.[48] Only a 2 ppt of NO_3 accounted for 40% of isoprene nitrate production in the late afternoon. However, the relative role of OH versus NO_3 oxidation on the production of daytime monoterpene nitrates is unknown. The campaign average steady state NO_3 concentration diurnal profile was estimated using eq 1, with $k_1 = 1.4 \times 10^{-13} \exp(-2470/T)$ and $k_5 = 1.8 \times 10^{-11} \exp(110/T)$[79] and is shown in Figure S5. J_{NO_3} values were estimated using the TUV model based on 1 day from the middle of each campaign.[80] During the summer campaign, the calculated NO_3 concentrations increased slightly throughout the morning and afternoon to ∼3 pptv, before a sharp increase during the late afternoon into the evening reaching ∼20 pptv, before a minimum around 08:00 of ∼0.1 pptv. The winter diurnal variation shows two peaks in NO_3 concentrations; the first peak around 04:00 at ∼2 pptv before a morning minimum and then another peak around 17:00−5 pptv in line with ozone concentrations. The average diurnal variation of the NOS_{MT} species, shown in Figure 2, is consistent with the calculated average NO_3 concentration profiles. However, no direct correlation was observed between the individual NOS_{MT} concentrations and concurrent NO_3 concentrations (R^2 < 0.2), likely due to the multigenerational and heterogeneous pathways of these tracers. Further work is needed to understand the factors controlling NOSMT in polluted areas during the day.

$$[NO_3] = \frac{k_1[O_3][NO_2]}{J_3 + J_4 + k_5[NO]} \quad (1)$$

Monoterpene Organosulfates (OS_{MT}). The identified monoterpene derived OSs (OS_{MT}) included 44 $C_{9/10}$ species during the summer and winter campaigns, as shown in Table 1. These OS_{MT} have been shown to be produced from either photooxidation or nitrate radical oxidation of monoterpene VOCs,[23,56] followed by reactive uptake or sulfate radical reaction.[29] Total OS_{MT} concentrations were roughly double during the winter (5.6 ± 0.8 ng m^{-3}) compared to those in the summer (2.4 ± 0.8 ng m^{-3}), similar to results seen in other areas in China.[6,73]

$C_9H_{16}O_6S$ was the most abundant OS_{MT} species during the summer with an average concentration of 0.9 ± 0.4 ng m^{-3}, with similar concentrations observed previously in Shanghai (1.17 ng m^{-3}).[6] Much lower concentrations were observed in Beijing (0.06 ng m^{-3}).[73] $C_{10}H_{16}O_5S$ was the second most abundant OS_{MT} species during the summer (0.46 ± 0.2 ng m^{-3}) and was previously identified in Denmark, with concentrations of 0.8 and 0.6 ng m^{-3} observed at urban and semirural sites, respectively.[40] The highest OS_{MT} concentration observed across either campaign was $C_9H_{16}O_7S$ during the winter, with a time averaged mean concentration of 2.72 ± 0.2

https://doi.org/10.1021/acsearthspacechem.1c00204
ACS Earth Space Chem. XXXX, XXX, XXX−XXX

Table 1. Molecular Formula, Retention Times, and Time Weighted Means (ng m^{-3}) of Nitrooxy Oganosulfates (NOS) and Organosulfates (OS) from Monoterpenes (MT) and Isoprene (i) Observed Across Summer and Winter Campaigns in Guangzhou[a]

molecular formula	summer concentration (ng m^{-3})	winter concentration (ng m^{-3})	retention time (min)
		NOS_{MT}	
$C_{10}H_{17}NO_7S$	7.15	11.11	9.40, 10.50, 11.27, 11.64, 11.97, 12.37, 13.10, 13.76
$C_{10}H_{17}NO_8S$	0.48	0.62	4.77, 4.98, 5.55, 5.98, 6.40, 6.97, 7.18, 8.39
$C_{10}H_{17}NO_9S$	0.31	0.42	3.84, 6.61, 8.50, 9.03, 10.47, 13.27, 17.55
$C_{10}H_{19}NO_9S$	0.04	0.05	5.55
$C_9H_{15}NO_8S$	0.37	0.91	3.41, 5.98
NOS_{MT} sum	8.34	13.10	
		OS_{MT}	
$C_{10}H_{16}O_5S$	0.46	0.83	2.88, 3.84, 4.87, 5.66, 7.18, 7.43, 8.39, 9.38, 10.51, 11.29, 11.75, 12.8, 13.76
$C_{10}H_{16}O_6S$	0.05	0.08	9.07, 10.47
$C_{10}H_{16}O_7S$	0.09	0.65	2.74, 3.7, 7.04, 12.06
$C_{10}H_{18}O_5S$	0.33	0.26	2.89, 3.37, 6.86
$C_{10}H_{18}O_6S$	0.16	0.17	3.41
$C_{10}H_{18}O_7S$	0.07	0.07	6.08, 7.43
$C_{10}H_{18}O_8S$	0.04	0.07	9.38, 10.51, 11.29, 11.75, 11.99, 12.38, 13.76
$C_9H_{16}O_6S$	0.90	0.74	2.86, 3.44, 6.90, 7.37, 7.74, 8.84
$C_9H_{16}O_7S$	0.32	2.72	1.72, 2.85, 3.41, 4.52, 6.68, 6.97
OS_{MT} sum	2.44	5.60	
		NOSi	
$C_5H_{10}O_{11}N_2S$	9.65	6.96	1.36, 1.68, 1.92, 2.95, 3.59
$C_5H_9O_{10}NS$	8.17	2.50	0.94
$C_5H_{11}O_9NS$	5.21	1.40	0.86
$C_5H_{11}O_8NS$	0.61	0.40	1.09
$C_5H_9O_{13}N_3S$	0.05	0.01	7.86, 8.22, 8.4
NOSi sum	23.68	11.27	
		OSi	
$C_5H_{12}O_7S$	57.42	4.79	0.71
$C_2H_4O_6S$	23.95	11.71	0.73
$C_8H_{14}O_6S$	13.47	10.94	1.48
		OSi	
$C_3H_6O_5S$	12.20	6.74	0.73
$C_4H_8O_7S$	11.84	5.71	0.73
$C_5H_8O_7S$	11.76	5.68	0.73
$C_5H_{10}O_7S$	11.44	5.02	0.73
$C_5H_{10}O_6S$	11.24	5.52	0.79
$C_4H_8O_6S$	10.85	5.41	0.74
$C_6H_{10}O_7S$	9.04	8.60	0.74
$C_5H_{10}O_5S$	8.00	19.53	0.93
$C_8H_{14}O_7S$	6.96	1.90	0.74
$C_8H_{12}O_7S$	5.79	2.52	0.74
$C_3H_6O_6S$	5.61	5.08	0.73
$C_2H_6O_5S$	5.13	9.26	0.73
$C_5H_{10}O_8S$	4.48	1.11	0.73
$C_2H_4O_5S$	4.28	3.10	0.73
$C_5H_8O_5S$	3.91	1.89	0.85
$C_4H_8O_5S$	3.36	3.73	0.75
$C_6H_{12}O_7S$	3.28	2.44	0.83
$C_8H_{14}O_8S$	2.62	1.97	0.74
$C_3H_6O_7S$	2.01	2.36	0.75
$C_5H_{12}O_6S$	1.67	1.04	0.74
$C_5H_8O_9S$	1.46	0.60	0.64
$C_4H_6O_6S$	1.41	2.66	0.74
$C_3H_8O_6S$	1.31	1.26	0.75
$C_7H_{10}O_6S$	0.87	0.89	0.74
$C_8H_{14}O_{10}S$	0.68	0.46	0.73
$C_8H_{10}O_4S$	0.01	0.30	0.78
isoprene OS	**236.07**	**132.20**	
OSi	181.79	69.45	
total BSOA	216.25	99.42	

[a]OSi species in bold had R correlation coefficients of less than 0.6 towards 2-MT-OS or 2-MG-OS and were therefore not used in the analysis of OSi formation. Isoprene OS is the sum of all potential isoprene OS species quantified in this study, while OSi is the sum of all isoprene OS species, which had an R of greater than 0.6 towards either 2-Mt-OS or 2-MG-OS. Total BSOA is the sum of all quantified markers in this study.

ng m^{-3}, similar to concentrations (2.5 ± 2.3 ng m^{-3}) observed at an urban site in Copenhagen, Denmark during the summer.[40] $C_9H_{16}O_7S$ showed the most prominent winter enhancement, with winter concentrations ~8 times higher than those observed in the summer.

As for the NOS_{MT}, many of the OS_{MT} species were only identified in a small number of the samples, and only tracers that were identified in at least 40% of the samples were used for analysis. Total OS_{MT} species identified showed nighttime enhancement with a minima during the afternoon, as shown in Figure 2c,d. This nighttime peak of OS_{MT} species is likely linked to the nighttime enhancements of precursor monoterpene concentrations.[76] Previous laboratory studies of monoterpenes with NO_3 radicals have also shown the formation of OS_{MT} with the same molecular formulas as measured here.[56] Interestingly, none of the OS_{MT} species showed a significant correlation (R^2 < 0.10) toward SO_4^{2-} across either campaign, although the highest OS_{MT} concentrations did generally occur under the highest SO_4^{2-} concentrations (Figure S3). SO_2 was measured during the winter campaign, but again no significant correlation (R^2 < 0.1) was observed toward the OS_{MT} tracers. Chamber studies have shown that, for the reactive uptake of monoterpene derived epoxides to acidic sulfate aerosol, extreme acidity levels typically not observed in ambient environment are required and as such is not thought to be a major route to OS_{MT} formation.[81] Much like the NOS_{MT} species, OS_{MT} showed no direct correlation toward NO_2 concentrations at any time of day (R^2 < 0.15), although higher daytime OS_{MT} concentrations were associated with higher NO_2 concentrations during both campaigns. Another potential route of formation could be the degradation of nitrates or NOS_{MT} species to OS_{MT} species through hydrolysis.[31,32] This is further evidenced by the strong correlation between NOS_{MT} and OS_{MT} concentrations (Figure S6) during the summer campaign (R^2 = 0.87), while a weaker correlation was observed in the winter (R^2 = 0.32), although

https://doi.org/10.1021/acsearthspacechem.1c00204
ACS Earth Space Chem. XXXX, XXX, XXX−XXX

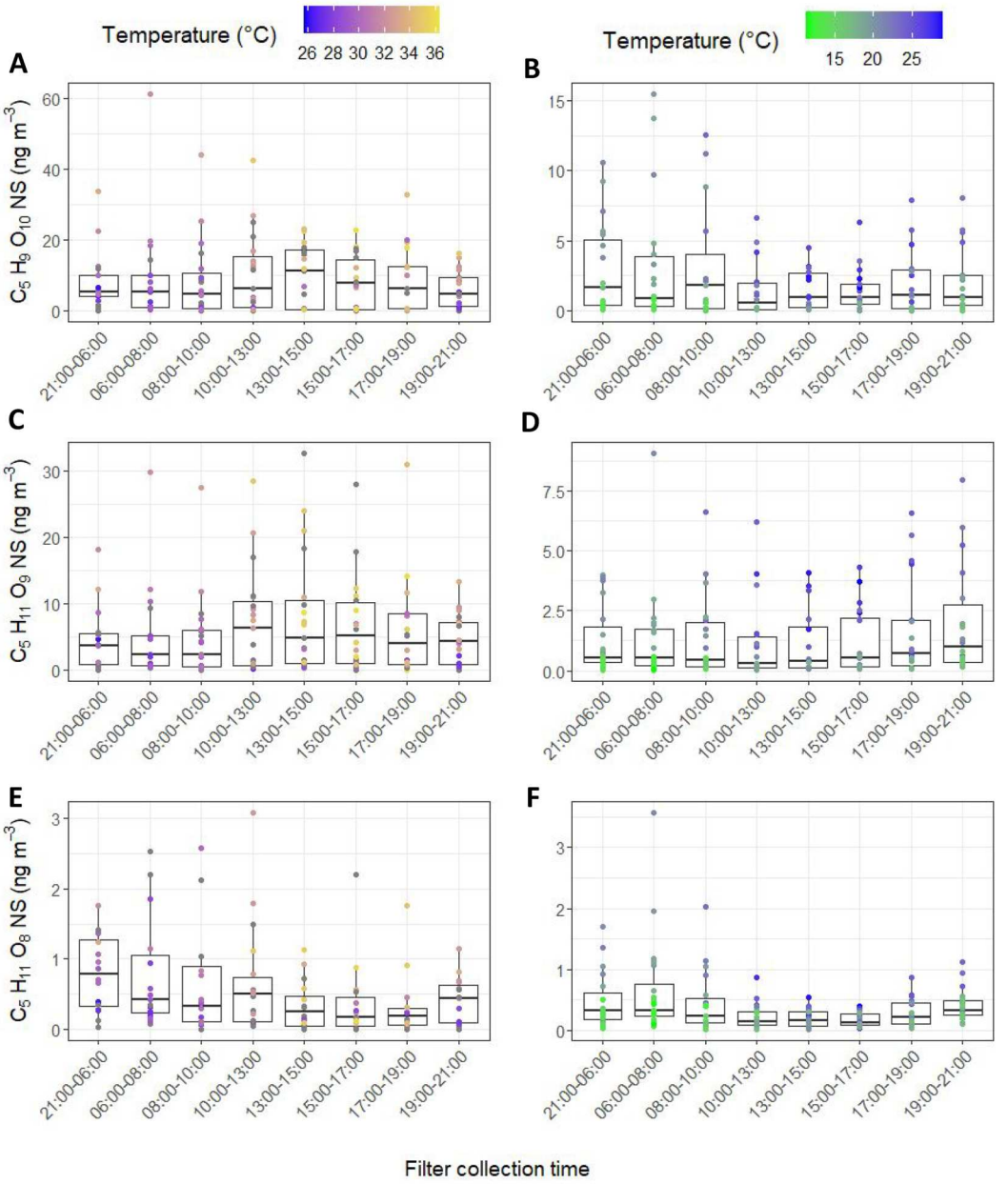

Figure 4. Diurnal variations of three mononitrated NOSi species across (A, C, and E) the summer (left) and (B, D, and F) the winter (right). Data points were then colored by the average temperature over the filter sampling time period. Where temperature measurements were not available, the data points are in gray.

no dependence on RH was observed in either campaign. Further work is needed to determine the hydrolysis pathways of these NOS_{MT} species leading to OS_{MT} in aqueous particles.

Isoprene Nitrooxy Organosulfates (NOSi). Eleven isoprene nitroxy organosulfate (NOSi) tracers were identified in the samples across the two campaigns, including mononitrated ($C_5H_9O_{10}NS$, $C_5H_{11}O_9NS$, $C_5H_{11}O_8NS$), dinitrated ($C_5H_{10}O_{11}N_2S$), and trinitrated ($C_5H_9O_{13}N_3S$) species. Unlike the NOS_{MT} species, NOSi concentrations were roughly double during the summer (23.7 ± 19.7 ng m $^{-3}$) than those in the winter (11.3 ± 10.2 ng m^{-3}), likely due to higher isoprene emissions. Three mononitrated species have been observed in ambient samples previously in Shanghai[6] and Beijing.[1,6,8,48] The most abundant mono-NOSi across both campaigns was $C_5H_9O_{10}NS$, with average concentrations of 8.2 ± 9.8 and 2.5 ± 3.0 ng m^{-3} across the summer and winter campaigns, respectively. This is consistent with previous summertime measurements in Beijing in 2015 (9.17 ng m^{-3})[1] and Shanghai, also for summers 2015 (2.14 ng m^{-3}) and 2019 (7.39 ng m^{-3}).[6] Interestingly Wang et al. in 2021 did not identify $C_5H_9O_{10}NS$ during the winter samples collected in Shanghai during 2016 and 2019. $C_5H_9O_{10}NS$ was first observed by Nestorowisz et al. in 2018 via smog chamber experiments and is suggested to form from the photo-oxidation of isoprene in the presence of NO. More recently, it has been suggested that it could be produced from the heterogeneous sulfate reaction with isoprene hydroxy-α-lactone species formed from the oxidation of isoprene nitroxy aldehyde by NO_3 or OH radicals.[46,82] The average diurnal variation of $C_5H_9O_{10}NS$ observed during the summer is almost flat, with a slight uptick

https://doi.org/10.1021/acsearthspacechem.1c00204
ACS Earth Space Chem. XXXX, XXX, XXX−XXX

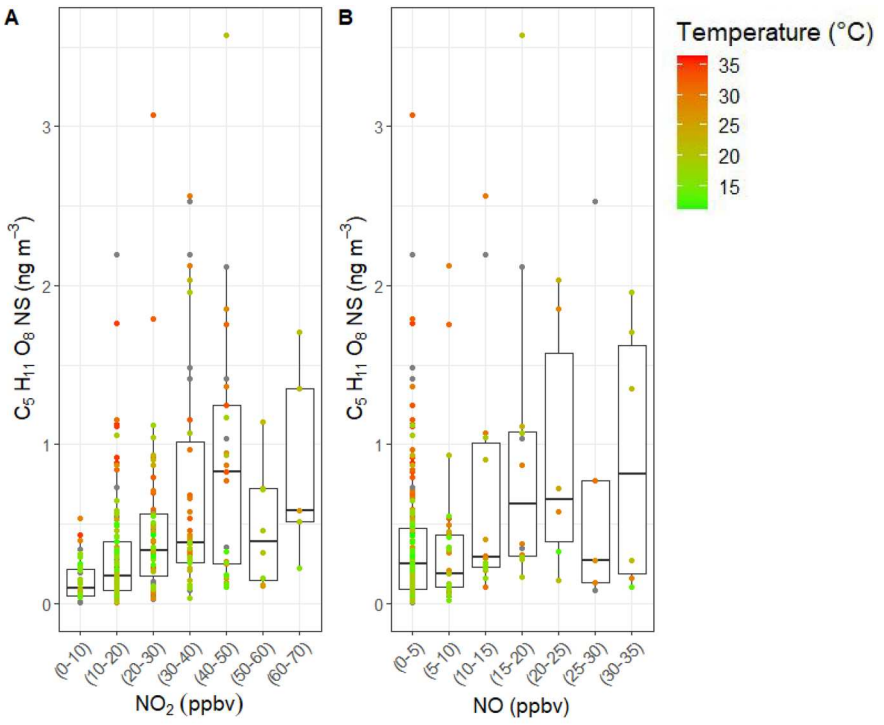

Figure 5. $C_5H_{11}O_8NS$ vs binned NO_X concentrations across both campaigns: (A) NO_2 and (B) NO. NO_2 concentrations were filtered to below 70 ppbv due to a limited number of data points. Data points were then colored by the average temperature over the filter sampling time period. Where temperature measurements were not available, the data points are in gray.

during the afternoon, in line with expected peak isoprene emissions, while in the winter, the diurnal variation showed enhancement during the night and early morning (Figure 4 a,b). The diurnal variations also highlight the temperature dependences of the concentrations, with the points colored by color, with overlapping temperature scales. During both campaigns, lower temperatures are associated with lower tracer concentrations. Lower isoprene concentrations are linked to lower temperatures, with this variation in isoprene emissions likely the driver for the limited diurnal variation. Strong correlations (R^2 = 0.61) toward inorganic sulfate were observed during the day during the summer campaign but no correlation occurred at night (R^2 = 0.16), while during the winter campaign, a weaker correlation was seen during the day (R^2 = 0.26) and similar correlation during the night (R^2 = 0.18). $C_5H_9O_{10}NS$ showed no direct correlation toward NO or NO_2 across the two campaigns (R^2 < 0.1). Overall, this suggests that particulate sulfate concentrations play a role in controlling in the formation of $C_5H_9O_{10}NS$, especially during the summer.

$C_5H_{11}O_9NS$ was the second most abundant of the mono-NOSi tracers, with summer and winter concentrations of 5.2 ± 7.0 and 1.4 ± 1.8 ng m^{-3}, compared to Beijing during the summer at 12.6 ng m^{-3}[1,48] and Shanghai at 6.82 and 0.24 ng m^{-3} during the summer and winter, respectively.[6] Hamilton et al. in 2021 proposed that this species is formed from the acid catalyzed heterogeneous uptake of isoprene nitroxy hydroxyepoxide via the initial NO_3 oxidation of isoprene. NO_3 oxidation is thought to be competitive with OH radicals in the formation of isoprene nitrates in Beijing during the afternoons as a result of low NO concentrations, similar to those observed in Guangzhou. The average diurnal profiles of $C_5H_{11}O_9NS$ during the summer and winter are shown in Figure 4c,d, respectively. During the summer, a slight increase in concentrations during the afternoon is observed, while during the winter, a slight increase is observed during the evening. No correlation was observed toward NO or NO_2 throughout either campaign, but a strong correlation toward particulate SO_4^{2-} (R^2 = 0.62) was observed in the summer daytime samples, compared to R^2 = 0.22 during the winter daytime.

In contrast to the other mono-NOSi species, $C_5H_{11}O_8NS$ showed similar concentrations during the summer and winter campaigns, with concentrations of 0.61 ± 0.6 and 0.4 ± 0.4 ng m^{-3}, respectively. $C_5H_{11}O_8NS$ showed the clearest nighttime enhancement across both campaigns, as shown in Figure 4e,f. $C_5H_{11}O_8NS$ was first identified by Surratt et al. in 2008 in chamber experiments and previously identified in Beijing during the summer with a lower mean concentration of 0.11 ng m^{-3}.[1] No studies to our knowledge have proposed a formation route for this species, with the species being identified in both isoprene/H_2O_2/NO/acidic seed and isoprene/HONO/neutral seed experiments. Unlike the other mono-NOSi species, $C_5H_{11}O_8NS$ showed a weak correlation toward sulfate, with the highest correlation observed during the summer daytimes (R^2 = 0.26). $C_5H_{11}O_8NS$ showed a limited direct correlation toward either NO or NO_2 mixing ratios. However, when the concentrations of $C_5H_{11}O_8NS$, across both campaigns were plotted against binned NO_2 (10 ppb bins size) and NO (5 ppb bin size), the average concentrations increased under more polluted conditions, as shown in Figure 5.

The dinitrate NOSi species ($C_5H_{10}O_{11}N_2S$) were identified across the summer (9.7 ± 6.3 ng m^{-3}) and winter (7.0 ± 6.5 ng m^{-3}) campaigns, with four isomers identified in the summer compared to five during the winter. The dominant isomer in terms of concentration eluted at 1.92 min and accounted for

https://doi.org/10.1021/acsearthspacechem.1c00204
ACS Earth Space Chem. XXXX, XXX, XXX−XXX

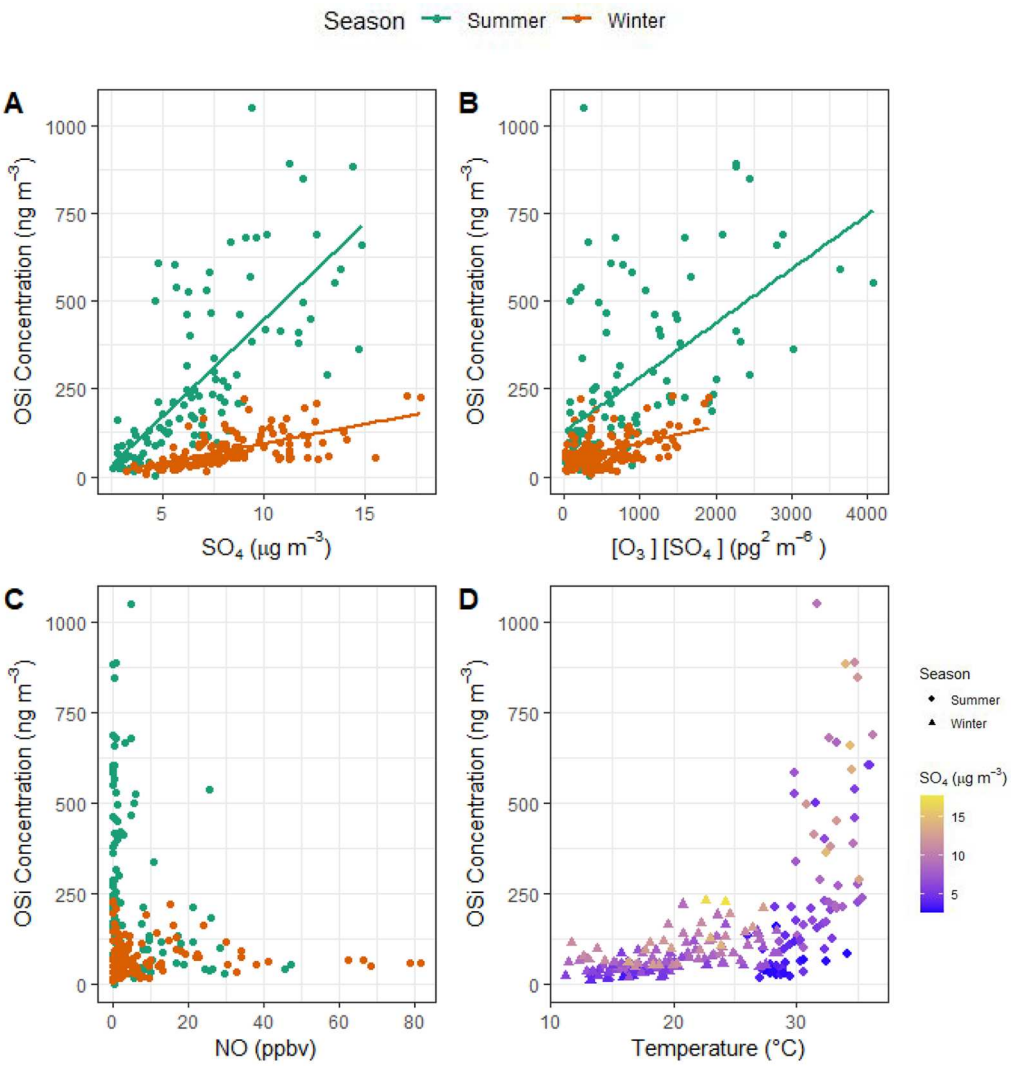

Figure 6. (A) Correlation between OSi concentrations and particulate sulfate, colored by season. (B) Correlation between OSi and the product of $[O_3][SO_4^{2-}]$, colored by season. (C) Correlation between OSi concentration and NO, colored by season. (D) Correlation between OSi and temperature across both campaigns, colored by SO_4^{2-} concentrations, with the shape indicating the campaign.

76% and 85% of the summer and winter total $C_5H_{10}O_{11}N_2S$ concentrations, respectively. Figure S7 shows the diurnal variations of the isomers, which were identified in at least one filter sample per collection period. The isomers generally show a clear nighttime enhancement, with a minimum during the afternoon, suggesting that nighttime formation is the dominant route. High variability in concentrations of the dinitrate NOSi were observed, most likely due to isoprene emission.

For the winter samples in Figure S7b,d, there is a clear temperature dependence in the concentrations observed. $C_5H_{10}O_{11}N_2S$ was first identified by Surratt et al. in 2008 via photo-oxidation in the presence of NO_X or nighttime NO_3 oxidation. $C_5H_{10}O_{11}N_2S$ was previously identified in Beijing, where four isomers were identified, with a strong nighttime enhancement and an average concentration of 2.6 ng m^{-3}.[1,48] Two dark NO_3 radical formation pathways have been proposed for this dinitrated species. Ng et al. in 2008 suggested formation via an isoprene hydroxynitrate from two subsequent NO_3 attacks, followed by reaction with sulfate.[47] Hamilton et al. in 2021 proposed a different route via heterogeneous uptake onto sulfate of a dinitrated epoxide species formed via two subsequent NO_3 radical additions. A daytime formation route has also been proposed via the photo-oxidation of isoprene in the presence of NO.[83] Figure S8 shows the concentrations of the two dominant $C_5H_{10}O_{11}N_2S$ isomers against binned NO_2 concentrations during the summer (left) and winter (right) and show general increases in concentration with increasing NO_2 levels. No correlation with NO or NO_3 concentrations was observed during either campaign. The lack of correlation toward NO_3 is likely due to the comparatively long lifetimes of the NOS species at night compared to NO_3 with NO_3 concentrations quickly dropping throughout the night during both campaigns. The $C_5H_{10}O_{11}N_2S$ markers also show high concentrations during the morning sample, under low NO_3 concentrations, likely due to nonlocal sources or boundary layer conditions. $C_5H_{10}O_{11}N_2S$ unlike the mononitrated species showed no correlation toward SO_4^{2-} during either campaign ($R^2 < 0.10$), suggesting that SO_4^{2-} is not a limiting reagent in the formation of this dinitrate, which has been observed previously in Beijing.[48] Overall, this suggests that $C_5H_{10}O_{11}N_2S$ is limited by the availability of NO_3 radicals rather than particulate sulfate concentrations, but further work is needed to understand the formation routes in the real atmosphere.

https://doi.org/10.1021/acsearthspacechem.1c00204
ACS Earth Space Chem. XXXX, XXX, XXX−XXX

Isoprene Organosulfates (OSi). Thirty-one OSi tracers were identified across the summer and winter (Table 1), while two OSi species were exclusively observed in the summer ($C_5H_{12}O_8S$ and $C_8H_{10}O_4S$) but were only minor components of the total summertime OSi concentrations (0.16%) and so were not considered further to allow for a direct comparison between the two seasons. Figures S9 and S10 show correlation plots (corPlot, Openair, R package) containing the OSi tracers from the summer and winter, respectively. The plots highlight the strong correlations between the species. The number represents the Pearson coefficient (R) between the two species, i.e., 60 is an R of 0.6. More elongated circles represent higher correlations either positive (to the right) or negative (to the left), while darker red circles represent higher positive correlations and lighter green/blue circles represent stronger negative correlations. In both campaigns, there are several tracers that have weaker correlations toward the rest of the tracers, which is more pronounced during the winter campaign, with $C_5H_{10}O_5S$ and $C_4H_6O_6S$ showing anticorrelations, suggesting a mixed biogenic/anthropogenic source. The two most well-studied isoprene tracers are $C_5H_{12}O_7S$ and $C_4H_8O_7S$. For quality control, OSi tracers that did not show a moderate (R > 0.60, as shown in Figures S9 and S10) correlation toward at least one of these tracers in either campaign were removed from the data set. This was done to improve the confidence that these tracers are from isoprene chemistry rather than other sources. Eighteen OSi tracers were therefore used in the analysis across both campaigns and going forward known collectively as OSi.

The most abundant tracer during the summer campaign was $C_5H_{12}O_7S$ (2-methyl tetrol organosulfate, 2-MT-OS) with an average concentration of 57.4 ± 90.4 ng m^{-3} accounting for 32% of the total OSi. Much lower concentrations of 2-MT-OS were seen during the winter campaign, with an average concentration of 4.8 ± 7.1 ng m^{-3} and a lower contribution (6.9%) to the total OSi concentration. 2-MT-OS is one of the most common isoprene tracers and has been identified in multiple locations globally, including China,[1,6,8] the US,[4,5,84] Europe,[40] and South America.[85] 2-MT-OS is formed via the reactive uptake of isoprene epoxydiols (IEPOX) with particulate sulfate and is often used as a marker of "low-NO" isoprene photochemistry.[27,63] $C_4H_8O_7S$ (2-methyl glyceric acid organosulfate, 2-MG-OS) is another common OSi tracer, formed via reactive uptake onto the sulfate of methacrylic acid epoxide (MAE) or hydroxymethyl−methyl lactone (HMML) via a "high NO" formation pathway.[14,27,86,87] 2-MG-OS showed less seasonality than 2-MT-OS with summer and winter concentrations of 11.8 ± 15.7 and 5.7 ± 4.9 ng m^{-3}, respectively. 2-MG-OS concentrations could be influenced by high average temperatures during both campaigns (summer, 30.4 °C; winter, 18 °C) due to the rapid thermolysis of peroxymethacryloyl (PMA), the precursor to methacryloylperoxynitrate (MPAN) above 20 °C.[88] During the summer, the average 2-MT-OS/2-MG-OS ratio was 7.6, with a maximum of 49.2, which occurred under low NO conditions for an urban area (ca. 0.48 ppb). Mean NO concentrations were roughly double during the winter (12.1 ppb) compared to those in the summer (5.37 ppb). The average 2-MT-OS/2-MG-OS ratio observed in summer was very similar to previous observations in Shanghai (6.8−7.8).[6] The largest observed 2-MT-OS/2-MG-OS ratios are in line with those seen in the southeastern United States (33.8).[4] During the winter, the average 2-MT-OS/2-MG-OS ratio was 0.73 (range 0.01−3.8). The lowest 2-MT-OS/2-MG-OS ratios occurred during the lowest NO concentrations, likely due to the extremely low afternoon NO concentrations and long sampling periods and were similar to those observed in summertime Beijing (0.55, Bryant et al. in 2020), suggesting that wintertime oxidation conditions in Guangzhou are similar to those during summer in Beijing. Newland et al. in 2021 showed that up to 30% of isoprene derived peroxy radicals (ISOPOO) from OH oxidation can react with HO_2 rather than NO during the afternoon in Beijing when NO concentrations drop to less than 1 ppb.

Strong correlations were observed between the majority of tracers identified as OSi (R = 0.50−0.97), as shown in Figures S9 and S10, indicating similar formation pathways or losses. The OSi tracers concentrations were summed to allow for an investigation of what influences OSi formation in Guangzhou. Total OSi concentrations showed moderate correlations toward particulate sulfate across both campaigns as shown in Figure 6a (summer, R^2 = 0.55; winter, R^2 = 0.40). Interestingly, the gradients of the best fits during the summer and winter are very different, with the summer gradient ∼6.7 times higher than that of the winter. During the summer, every additional 1 μg m^{-3} of sulfate available increases the OSi concentrations by ∼52 ng m^{-3} but only 7.7 ng m^{-3} in the winter. Bryant et al. in 2020 showed a stronger correlation between OSi species with the product of ozone (as a proxy for photochemistry) and particulate sulfate in Beijing, highlighting the role of both local photochemistry and particulate sulfate in OSi formation. However, in Guangzhou, the correlation of total OSi concentrations toward $[O_3][SO_4^{2-}]$ were lower (summer R^2 = 0.32 and winter R^2 = 0.20) than the correlations toward sulfate (Figure 6b). The correlation of $[O_3][SO_4^{2-}]$ is likely to be weaker at longer photochemical ages when the O_3 concentration is not directly related to the photochemical formation of the OSi local to the observation site. During the summer, the highest total OSi concentrations occurred under the lowest NO concentrations (0−5 ppb, Figure 6b), highlighting the importance of "low-NO" oxidation routes for isoprene emissions during the summer.

The OSi tracers showed strong seasonality in comparison to the other tracer groups, with average summer and winter concentrations of 181.8 (1.84−1049.8 ng m^{-3}) and 69.5 ng m^{-3} (7.8−229.4 ng m^{-3}), respectively. This large difference in concentrations is likely due to both changes in isoprene emissions,[65] and solar irradiance and has been observed at other locations.[6,41]

OSi concentrations greatly increased with temperature above 30 °C, as shown in Figure 6d. This type of temperature dependence has been seen for isoprene emissions previously.[80,89] Overall, this suggests that increased OSi concentrations are driven by primary isoprene emissions as well as the availability of sulfate for uptake into the particle phase.

CONCLUSION

$PM_{2.5}$ filter collection was conducted to investigate the formation processes of organosulfates (OSs) and nitrooxy-organosulfates (NOSs) across a summer and winter campaign in Guangzhou, a southern Chinese megacity, influenced by high biogenic and anthropogenic emissions. The targeted analysis of OSs and NOSs from isoprene and monoterpenes was undertaken, with tracers quantified using both authentic and proxy standards. Quantified biogenic OS and NOS concentrations averaged 216.3 and 99.4 ng m^{-3} during the summer and winter, respectively, with OSi contributing 84%

https://doi.org/10.1021/acsearthspacechem.1c00204
ACS Earth Space Chem. XXXX, XXX, XXX−XXX

and 70%. The majority of monoterpene derived OS and NOS species showed strong nocturnal enhancements, owing to increased precursor emissions and/or NO_3 oxidation chemistry. OS_{MT} showed a limited correlation to potential reactants but showed a strong correlation toward NOS_{MT} species, especially during the summer, suggesting a potential NOS_{MT} to OS_{MT} degradation route. Several NOSi species were identified, with mixed formation routes via both daytime OH and ozone initiated photo-oxidation and nocturnal NO_3 oxidation. Several of the mononitrated species showed moderate correlations to particulate sulfate (R^2 = 0.61), while the dinitrated species were poorly correlated (R^2 < 0.1). 2-MT-OS was the most abundant isoprene tracer during the summer campaign, with an average concentration of 57.4 ng m^{-3}, 32% of the total OSi. 2-MT-OS/2-MG-OS ratios during the summer (7.6) compared to those in the winter (0.73) suggest that low-NO formation pathways were dominant in the summer, as seen in Beijing previously. OSi species showed a strong temperature dependence, with concentrations increasing sharply with temperatures above 30 °C, likely due to increased precursor isoprene emissions. OSi showed a direct relationship toward particulate sulfate, especially during the summer and highlights the extensive heterogeneous chemistry occurring. Future studies should focus on increasing the time resolution of observations of OS/NOS, taken alongside detailed speciated VOC measurements and NO_3 radical measurements, to allow for more detailed diurnal variations to be studied as well as improving our ability to accurately quantify tracers through the synthesis of standards or new quantification techniques.

■ ASSOCIATED CONTENT

Supporting Information

The Supporting Information is available free of charge at https://pubs.acs.org/doi/10.1021/acsearthspacechem.1c00204.

> Tables of measured matrix effects of eight ambient filter samples and overview of measured meteorological parameters and pollutants and figures of diurnal variations of measured meteorological parameters and pollutants, time series and diurnal variation of SO_2, correlation between monoterpene derived species and inorganic sulfate, correlation between monoterpene derived nitrooxy organosulfates and NO_2, diurnal variations of steady state NO_3 concentrations, correlation between monoterpene derived organosulfates and nitrooxy organosulfates, diurnal variation of dinitrated isoprene nitrooxy organosulfate sulfates, correlation between dinitrated isoprene nitrooxy organosulfate and NO_2, correlations between measured isoprene organosulfates during the summer campaign, and correlations between measured isoprene organosulfates during the winter campaign (PDF)

■ AUTHOR INFORMATION

Corresponding Author

Daniel J. Bryant − *Wolfson Atmospheric Chemistry Laboratories, University of York, York YO10 5DD, United Kingdom;* orcid.org/0000-0001-6605-6136; Email: djb561@york.ac.uk

Authors

Atallah Elzein − *Centre for Radiation Chemical and Environmental Hazards, Toxicology Department, Public Health England, Didcot OX11 0RQ, United Kingdom*

Mike Newland − *Institut de Combustion, Aérothermique, Réactivité et Environnement (ICARE), CNRS (UPR 3021), Orléans Cedex 2 45071 Centre-Val de Loire, France*

Erin White − *Wolfson Atmospheric Chemistry Laboratories, University of York, York YO10 5DD, United Kingdom*

Stefan Swift − *Wolfson Atmospheric Chemistry Laboratories, University of York, York YO10 5DD, United Kingdom*

Amy Watkins − *Wolfson Atmospheric Chemistry Laboratories, University of York, York YO10 5DD, United Kingdom*

Wei Deng − *State Key Laboratory of Organic Geochemistry, Guangzhou Institute of Geochemistry, Guangzhou, Guangdong 510640, China*

Wei Song − *State Key Laboratory of Organic Geochemistry, Guangzhou Institute of Geochemistry, Guangzhou, Guangdong 510640, China*

Sainan Wang − *Chongqing Institute of Green and Intelligent Technology, Chongqing, Sichuan 401122, China;* orcid.org/0000-0002-5759-1484

Yanli Zhang − *State Key Laboratory of Organic Geochemistry, Guangzhou Institute of Geochemistry, Guangzhou, Guangdong 510640, China;* orcid.org/0000-0003-0614-2096

Xinming Wang − *State Key Laboratory of Organic Geochemistry, Guangzhou Institute of Geochemistry, Guangzhou, Guangdong 510640, China;* orcid.org/0000-0002-1982-0928

Andrew R. Rickard − *Wolfson Atmospheric Chemistry Laboratories, University of York, York YO10 5DD, United Kingdom; National Centre for Atmospheric Science, University of York, York YO10 5DD, United Kingdom*

Jacqueline F. Hamilton − *Wolfson Atmospheric Chemistry Laboratories, University of York, York YO10 5DD, United Kingdom;* orcid.org/0000-0003-0975-4311

Complete contact information is available at: https://pubs.acs.org/10.1021/acsearthspacechem.1c00204

Funding

This project was funded by the Natural Environmental Research Council (NE/S006648/1) and the Department of Science and Technology of Guangdong Province (Grant No. 2020B1212060053/2019B121205006). D.B. and S.S. acknowledge NERC SPHERES Ph.D. studentships. The Orbitrap-MS was funded by a Natural Environment Research Council strategic capital grant, CC090.

Notes

The authors declare no competing financial interest.

■ REFERENCES

(1) Bryant, D. J.; Dixon, W. J.; Hopkins, J. R.; Dunmore, R. E.; Pereira, K. L.; Shaw, M.; Squires, F. A.; Bannan, T. J.; Mehra, A.; Worrall, S. D.; Bacak, A.; Coe, H.; Percival, C. J.; Whalley, L. K.; Heard, D. E.; Slater, E. J.; Ouyang, B.; Cui, T.; Surratt, J. D.; Liu, D.; Shi, Z.; Harrison, R.; Sun, Y.; Xu, W.; Lewis, A. C.; Lee, J. D.; Rickard, A. R.; Hamilton, J. F. Strong Anthropogenic Control of Secondary Organic Aerosol Formation from Isoprene in Beijing. *Atmos. Chem. Phys.* **2020**, *20* (12), 7531−7552.

(2) Riva, M.; Da Silva Barbosa, T.; Lin, Y.-H.; Stone, E. A.; Gold, A.; Surratt, J. D. Chemical Characterization of Organosulfates in

Secondary Organic Aerosol Derived from the Photooxidation of Alkanes. *Atmos. Chem. Phys.* **2016**, *16* (17), 11001−11018.
(3) Wang, X.; Hayeck, N.; Brüggemann, M.; Yao, L.; Chen, H.; Zhang, C.; Emmelin, C.; Chen, J.; George, C.; Wang, L. Chemical Characteristics of Organic Aerosols in Shanghai: A Study by Ultrahigh-Performance Liquid Chromatography Coupled With Orbitrap Mass Spectrometry. *J. Geophys. Res. Atmos.* **2017**, *122* (21), 11703−11722.
(4) Hettiyadura, A. P. S.; Al-Naiema, I. M.; Hughes, D. D.; Fang, T.; Stone, E. A. Organosulfates in Atlanta, Georgia: Anthropogenic Influences on Biogenic Secondary Organic Aerosol Formation. *Atmos. Chem. Phys.* **2019**, *19* (5), 3191−3206.
(5) Budisulistiorini, S. H.; Li, X.; Bairai, S. T.; Renfro, J.; Liu, Y.; Liu, Y. J.; McKinney, K. A.; Martin, S. T.; McNeill, V. F.; Pye, H. O. T.; Nenes, A.; Neff, M. E.; Stone, E. A.; Mueller, S.; Knote, C.; Shaw, S. L.; Zhang, Z.; Gold, A.; Surratt, J. D. Examining the Effects of Anthropogenic Emissions on Isoprene-Derived Secondary Organic Aerosol Formation during the 2013 Southern Oxidant and Aerosol Study (SOAS) at the Look Rock, Tennessee Ground Site. *Atmos. Chem. Phys.* **2015**, *15* (15), 8871−8888.
(6) Wang, Y.; Zhao, Y.; Wang, Y.; Yu, J. Z.; Shao, J.; Liu, P.; Zhu, W.; Cheng, Z.; Li, Z.; Yan, N.; Xiao, H. Organosulfates in Atmospheric Aerosols in Shanghai, China: Seasonal and Interannual Variability, Origin, and Formation Mechanisms. *Atmos. Chem. Phys.* **2021**, *21* (4), 2959−2980.
(7) Iinuma, Y.; Böge, O.; Kahnt, A.; Herrmann, H. Laboratory Chamber Studies on the Formation of Organosulfates from Reactive Uptake of Monoterpene Oxides. *Phys. Chem. Chem. Phys.* **2009**, *11* (36), 7985−7997.
(8) Wang, Y.; Hu, M.; Guo, S.; Wang, Y.; Zheng, J.; Yang, Y.; Zhu, W.; Tang, R.; Li, X.; Liu, Y.; Le Breton, M.; Du, Z.; Shang, D.; Wu, Y.; Wu, Z.; Song, Y.; Lou, S.; Hallquist, M.; Yu, J. The Secondary Formation of Organosulfates under Interactions between Biogenic Emissions and Anthropogenic Pollutants in Summer in Beijing. *Atmos. Chem. Phys.* **2018**, *18* (14), 10693−10713.
(9) Kristensen, K.; Glasius, M. Organosulfates and Oxidation Products from Biogenic Hydrocarbons in Fine Aerosols from a Forest in North West Europe during Spring. *Atmos. Environ.* **2011**, *45* (27), 4546−4556.
(10) Brüggemann, M.; van Pinxteren, D.; Wang, Y.; Yu, J. Z.; Herrmann, H. Quantification of Known and Unknown Terpenoid Organosulfates in PM10 Using Untargeted LC−HRMS/MS: Contrasting Summertime Rural Germany and the North China Plain. *Environ. Chem.* **2019**, *16* (5), 333.
(11) Froyd, K. D.; Murphy, S. M.; Murphy, D. M.; De Gouw, J. A.; Eddingsaas, N. C.; Wennberg, P. O. Contribution of Isoprene-Derived Organosulfates to Free Tropospheric Aerosol Mass. *Proc. Natl. Acad. Sci. U. S. A.* **2010**, *107* (50), 21360−21365.
(12) Huang, R.-J.; Zhang, Y.; Bozzetti, C.; Ho, K.-F.; Cao, J.-J.; Han, Y.; Daellenbach, K. R.; Slowik, J. G.; Platt, S. M.; Canonaco, F.; Zotter, P.; Wolf, R.; Pieber, S. M.; Bruns, E. A.; Crippa, M.; Ciarelli, G.; Piazzalunga, A.; Schwikowski, M.; Abbaszade, G.; Schnelle-Kreis, J.; Zimmermann, R.; An, Z.; Szidat, S.; Baltensperger, U.; Haddad, I. El; Prévôt, A. S. H. High Secondary Aerosol Contribution to Particulate Pollution during Haze Events in China. *Nature* **2014**, *514* (7521), 218−222.
(13) Brüggemann, M.; Xu, R.; Tilgner, A.; Kwong, K. C.; Mutzel, A.; Poon, H. Y.; Otto, T.; Schaefer, T.; Poulain, L.; Chan, M. N.; Herrmann, H. Organosulfates in Ambient Aerosol: State of Knowledge and Future Research Directions on Formation, Abundance, Fate, and Importance. *Environ. Sci. Technol.* **2020**, *54*, 3767−3782.
(14) Lin, Y. H.; Zhang, H.; Pye, H. O. T.; Zhang, Z.; Marth, W. J.; Park, S.; Arashiro, M.; Cui, T.; Budisulistiorini, S. H.; Sexton, K. G.; Vizuete, W.; Xie, Y.; Luecken, D. J.; Piletic, I. R.; Edney, E. O.; Bartolotti, L. J.; Gold, A.; Surratt, J. D. Epoxide as a Precursor to Secondary Organic Aerosol Formation from Isoprene Photooxidation in the Presence of Nitrogen Oxides. *Proc. Natl. Acad. Sci. U. S. A.* **2013**, *110* (17), 6718−6723.
(15) Sheesley, R. J.; Kirillova, E.; Andersson, A.; Krusa, M.; Praveen, P. S.; Budhavant, K.; Safai, P. D.; Rao, P. S. P.; Gustafsson, O. Year-Round Radiocarbon-Based Source Apportionment of Carbonaceous Aerosols at Two Background Sites in South Asia. *J. Geophys. Res. Atmos.* **2012**, *117* (10), D10202.
(16) Kirillova, E. N.; Andersson, A.; Tiwari, S.; Srivastava, A. K.; Bisht, D. S.; Gustafsson, Ö. Water-Soluble Organic Carbon Aerosols during a Full New Delhi Winter: Isotope-Based Source Apportionment and Optical Properties. *J. Geophys. Res. Atmos.* **2014**, *119* (6), 3476−3485.
(17) Kirillova, E. N.; Andersson, A.; Sheesley, R. J.; Kruså, M.; Praveen, P. S.; Budhavant, K.; Safai, P. D.; Rao, P. S. P.; Gustafsson, Ö. ^{13}C- and ^{14}C-Based Study of Sources and Atmospheric Processing of Water-Soluble Organic Carbon (WSOC) in South Asian Aerosols. *J. Geophys. Res. Atmos.* **2013**, *118* (2), 614−626.
(18) Zhang, Y.; Ren, H.; Sun, Y.; Cao, F.; Chang, Y.; Liu, S.; Lee, X.; Agrios, K.; Kawamura, K.; Liu, D.; Ren, L.; Du, W.; Wang, Z.; Prévôt, A. S. H.; Szidat, S.; Fu, P. High Contribution of Nonfossil Sources to Submicrometer Organic Aerosols in Beijing, China. *Environ. Sci. Technol.* **2017**, *51* (14), 7842−7852.
(19) Kirillova, E. N.; Sheesley, R. J.; Andersson, A.; Gustafsson, Ö. Natural Abundance ^{13}C and ^{14}C Analysis of Water-Soluble Organic Carbon in Atmospheric Aerosols. *Anal. Chem.* **2010**, *82* (19), 7973−7978.
(20) Gómez-González, Y.; Surratt, J. D.; Cuyckens, F.; Szmigielski, R.; Vermeylen, R.; Jaoui, M.; Lewandowski, M.; Offenberg, J. H.; Kleindienst, T. E.; Edney, E. O.; Blockhuys, F.; Van Alsenoy, C.; Maenhaut, W.; Claeys, M. Characterization of Organosulfates from the Photooxidation of Isoprene and Unsaturated Fatty Acids in Ambient Aerosol Using Liquid Chromatography - Electrospray Ionization Mass Spectrometry. *J. Mass Spectrom.* **2008**, *43* (3), 371−382.
(21) Surratt, J. D.; Gómez-González, Y.; Chan, A. W. H.; Vermeylen, R.; Shahgholi, M.; Kleindienst, T. E.; Edney, E. O.; Offenberg, J. H.; Lewandowski, M.; Jaoui, M.; Maenhaut, W.; Claeys, M.; Flagan, R. C.; Seinfeld, J. H. Organosulfate Formation in Biogenic Secondary Organic Aerosol. *J. Phys. Chem. A* **2008**, *112* (36), 8345−8378.
(22) Surratt, J. D.; Murphy, S. M.; Kroll, J. H.; Ng, N. L.; Hildebrandt, L.; Sorooshian, A.; Szmigielski, R.; Vermeylen, R.; Maenhaut, W.; Claeys, M.; Flagan, R. C.; Seinfeld, J. H. Chemical Composition of Secondary Organic Aerosol Formed from the Photooxidation of Isoprene. *J. Phys. Chem. A* **2006**, *110* (31), 9665−9690.
(23) Chan, M. N.; Surratt, J. D.; Chan, A. W. H.; Schilling, K.; Offenberg, J. H.; Lewandowski, M.; Edney, E. O.; Kleindienst, T. E.; Jaoui, M.; Edgerton, E. S.; Tanner, R. L.; Shaw, S. L.; Zheng, M.; Knipping, E. M.; Seinfeld, J. H. Influence of Aerosol Acidity on the Chemical Composition of Secondary Organic Aerosol from β-Caryophyllene. *Atmos. Chem. Phys.* **2011**, *11* (4), 1735−1751.
(24) Shalamzari, M. S.; Vermeylen, R.; Blockhuys, F.; Kleindienst, T. E.; Lewandowski, M.; Szmigielski, R.; Rudzinski, K. J.; Spólnik, G.; Danikiewicz, W.; Maenhaut, W.; Claeys, M. Characterization of Polar Organosulfates in Secondary Organic Aerosol from the Unsaturated Aldehydes 2-E-Pentenal, 2-E-Hexenal, and 3-Z-Hexenal. *Atmos. Chem. Phys.* **2016**, *16* (11), 7135−7148.
(25) Xu, L.; Guo, H.; Boyd, C. M.; Klein, M.; Bougiatioti, A.; Cerully, K. M.; Hite, J. R.; Isaacman-VanWertz, G.; Kreisberg, N. M.; Knote, C.; Olson, K.; Koss, A.; Goldstein, A. H.; Hering, S. V.; Gouw, J. de; Baumann, K.; Lee, S.-H.; Nenes, A.; Weber, R. J.; Ng, N. L. Effects of Anthropogenic Emissions on Aerosol Formation from Isoprene and Monoterpenes in the Southeastern United States. *Proc. Natl. Acad. Sci. U. S. A.* **2015**, *112* (1), 37−42.
(26) Surratt, J. D.; Kroll, J. H.; Kleindienst, T. E.; Edney, E. O.; Claeys, M.; Sorooshian, A.; Ng, N. L.; Offenberg, J. H.; Lewandowski, M.; Jaoui, M.; Flagan, R. C.; Seinfeld, J. H. Evidence for Organosulfates in Secondary Organic Aerosol. *Environ. Sci. Technol.* **2007**, *41* (2), 517−527.
(27) Surratt, J. D.; Chan, A. W. H.; Eddingsaas, N. C.; Chan, M.; Loza, C. L.; Kwan, A. J.; Hersey, S. P.; Flagan, R. C.; Wennberg, P. O.;

https://doi.org/10.1021/acsearthspacechem.1c00204
ACS Earth Space Chem. XXXX, XXX, XXX−XXX

Seinfeld, J. H. Reactive Intermediates Revealed in Secondary Organic Aerosol Formation from Isoprene. *Proc. Natl. Acad. Sci. U. S. A.* **2010**, *107* (15), 6640−6645.
(28) Iinuma, Y.; Müller, C.; Berndt, T.; Böge, O.; Claeys, M.; Herrmann, H. Evidence for the Existence of Organosulfates from β-Pinene Ozonolysis in Ambient Secondary Organic Aerosol. *Environ. Sci. Technol.* **2007**, *41* (19), 6678−6683.
(29) Nozière, B.; Ekström, S.; Alsberg, T.; Holmström, S. Radical-Initiated Formation of Organosulfates and Surfactants in Atmospheric Aerosols. *Geophys. Res. Lett.* **2010**, *37* (5), L05806.
(30) Schindelka, J.; Iinuma, Y.; Hoffmann, D.; Herrmann, H. Sulfate Radical-Initiated Formation of Isoprene-Derived Organosulfates in Atmospheric Aerosols. *Faraday Discuss.* **2013**, *165* (0), 237−259.
(31) Darer, A. I.; Cole-Filipiak, N. C.; O'Connor, A. E.; Elrod, M. J. Formation and Stability of Atmospherically Relevant Isoprene-Derived Organosulfates and Organonitrates. *Environ. Sci. Technol.* **2011**, *45* (5), 1895−1902.
(32) Hu, K. S.; Darer, A. I.; Elrod, M. J. Thermodynamics and Kinetics of the Hydrolysis of Atmospherically Relevant Organonitrates and Organosulfates. *Atmos. Chem. Phys.* **2011**, *11* (16), 8307−8320.
(33) Passananti, M.; Kong, L.; Shang, J.; Dupart, Y.; Perrier, S.; Chen, J.; Donaldson, D. J.; George, C. Organosulfate Formation through the Heterogeneous Reaction of Sulfur Dioxide with Unsaturated Fatty Acids and Long-Chain Alkenes. *Angew. Chem., Int. Ed.* **2016**, *55* (35), 10336−10339.
(34) Kristensen, K.; Bilde, M.; Aalto, P. P.; Petäjä, T.; Glasius, M. Denuder/Filter Sampling of Organic Acids and Organosulfates at Urban and Boreal Forest Sites: Gas/Particle Distribution and Possible Sampling Artifacts. *Atmos. Environ.* **2016**, *130*, 36−53.
(35) Brüggemann, M.; Riva, M.; Perrier, S.; Poulain, L.; George, C.; Herrmann, H. Overestimation of Monoterpene Organosulfate Abundance in Aerosol Particles by Sampling in the Presence of SO_2. *Environ. Sci. Technol. Lett.* **2021**, *8*, 206−211.
(36) Kristensen, K.; Glasius, M. Organosulfates and Oxidation Products from Biogenic Hydrocarbons in Fine Aerosols from a Forest in North West Europe during Spring. *Atmos. Environ.* **2011**, *45* (27), 4546−4556.
(37) Wang, K.; Zhang, Y.; Huang, R. J.; Cao, J.; Hoffmann, T. UHPLC-Orbitrap Mass Spectrometric Characterization of Organic Aerosol from a Central European City (Mainz, Germany) and a Chinese Megacity (Beijing). *Atmos. Environ.* **2018**, *189*, 22−29.
(38) Le Breton, M.; Wang, Y.; Hallquist, Å. M.; Pathak, R. K.; Zheng, J.; Yang, Y.; Shang, D.; Glasius, M.; Bannan, T. J.; Liu, Q.; Chan, C. K.; Percival, C. J.; Zhu, W.; Lou, S.; Topping, D.; Wang, Y.; Yu, J.; Lu, K.; Guo, S.; Hu, M.; Hallquist, M. Online Gas- and Particle-Phase Measurements of Organosulfates, Organosulfonates and Nitrooxy Organosulfates in Beijing Utilizing a FIGAERO ToF-CIMS. *Atmos. Chem. Phys.* **2018**, *18* (14), 10355−10371.
(39) Wang, X. K.; Rossignol, S.; Ma, Y.; Yao, L.; Wang, M. Y.; Chen, J. M.; George, C.; Wang, L. Molecular Characterization of Atmospheric Particulate Organosulfates in Three Megacities at the Middle and Lower Reaches of the Yangtze River. *Atmos. Chem. Phys.* **2016**, *16* (4), 2285−2298.
(40) Nguyen, Q. T.; Christensen, M. K.; Cozzi, F.; Zare, A.; Hansen, A. M. K.; Kristensen, K.; Tulinius, T. E.; Madsen, H. H.; Christensen, J. H.; Brandt, J.; Massling, A.; Nøjgaard, J. K.; Glasius, M. Understanding the Anthropogenic Influence on Formation of Biogenic Secondary Organic Aerosols in Denmark via Analysis of Organosulfates and Related Oxidation Products. *Atmos. Chem. Phys.* **2014**, *14* (17), 8961−8981.
(41) He, Q. F.; Ding, X.; Wang, X. M.; Yu, J. Z.; Fu, X. X.; Liu, T. Y.; Zhang, Z.; Xue, J.; Chen, D. H.; Zhong, L. J.; Donahue, N. M. Organosulfates from Pinene and Isoprene over the Pearl River Delta, South China: Seasonal Variation and Implication in Formation Mechanisms. *Environ. Sci. Technol.* **2014**, *48*, 9236.
(42) Hansen, A. M. K.; Kristensen, K.; Nguyen, Q. T.; Zare, A.; Cozzi, F.; Nøjgaard, J. K.; Skov, H.; Brandt, J.; Christensen, J. H.; Ström, J.; Tunved, P.; Krejci, R.; Glasius, M. Organosulfates and Organic Acids in Arctic Aerosols: Speciation, Annual Variation and Concentration Levels. *Atmos. Chem. Phys.* **2014**, *14* (15), 7807−7823.
(43) Kahnt, A.; Behrouzi, S.; Vermeylen, R.; Safi Shalamzari, M.; Vercauteren, J.; Roekens, E.; Claeys, M.; Maenhaut, W. One-Year Study of Nitro-Organic Compounds and Their Relation to Wood Burning in PM10 Aerosol from a Rural Site in Belgium. *Atmos. Environ.* **2013**, *81*, 561−568.
(44) Eddingsaas, N. C.; Loza, C. L.; Yee, L. D.; Chan, M.; Schilling, K. A.; Chhabra, P. S.; Seinfeld, J. H.; Wennberg, P. O. α-Pinene Photooxidation under Controlled Chemical Conditions-Part 2: SOA Yield and Composition in Low-and High-NO_x Environments. *Atmos. Chem. Phys.* **2012**, *12* (16), 7413−7427.
(45) Ng, N. L.; Brown, S. S.; Archibald, A. T.; Atlas, E.; Cohen, R. C.; Crowley, J. N.; Day, D. A.; Donahue, N. M.; Fry, J. L.; Fuchs, H.; Griffin, R. J.; Guzman, M. I.; Herrmann, H.; Hodzic, A.; Iinuma, Y.; Jimenez, J. L.; Kiendler-Scharr, A.; Lee, B. H.; Luecken, D. J.; Mao, J.; McLaren, R.; Mutzel, A.; Osthoff, H. D.; Ouyang, B.; Picquet-Varrault, B.; Platt, U.; Pye, H. O. T.; Rudich, Y.; Schwantes, R. H.; Shiraiwa, M.; Stutz, J.; Thornton, J. A.; Tilgner, A.; Williams, B. J.; Zaveri, R. A. Nitrate Radicals and Biogenic Volatile Organic Compounds: Oxidation, Mechanisms, and Organic Aerosol. *Atmos. Chem. Phys.* **2017**, *17* (3), 2103−2162.
(46) Schwantes, R. H.; Teng, A. P.; Nguyen, T. B.; Coggon, M. M.; Crounse, J. D.; St. Clair, J. M.; Zhang, X.; Schilling, K. A.; Seinfeld, J. H.; Wennberg, P. O. Isoprene NO_3 Oxidation Products from the RO_2 + HO_2 Pathway. *J. Phys. Chem. A* **2015**, *119* (40), 10158−10171.
(47) Ng, N. L.; Kwan, A. J.; Surratt, J. D.; Chan, A. W. H.; Chhabra, P. S.; Sorooshian, A.; Pye, H. O. T.; Crounse, J. D.; Wennberg, P. O.; Flagan, R. C.; Seinfeld, J. H. Secondary Organic Aerosol (SOA) Formation from Reaction of Isoprene with Nitrate Radicals (NO_3). *Atmos. Chem. Phys.* **2008**, *8* (14), 4117−4140.
(48) Hamilton, J. F.; Bryant, D. J.; Edwards, P. M.; Ouyang, B.; Bannan, T. J.; Mehra, A.; Mayhew, A. W.; Hopkins, J. R.; Dunmore, R. E.; Squires, F. A.; Lee, J. D.; Newland, M. J.; Worrall, S. D.; Bacak, A.; Coe, H.; Percival, C.; Whalley, L. K.; Heard, D. E.; Slater, E. J.; Jones, R. L.; Cui, T.; Surratt, J. D.; Reeves, C. E.; Mills, G. P.; Grimmond, S.; Sun, Y.; Xu, W.; Shi, Z.; Rickard, A. R. Key Role of NO_3 Radicals in the Production of Isoprene Nitrates and Nitrooxyorganosulfates in Beijing. *Environ. Sci. Technol.* **2021**, *55* (2), 842−853.
(49) Liebmann, J.; Sobanski, N.; Schuladen, J.; Karu, E.; Hellen, H.; Hakola, H.; Zha, Q.; Ehn, M.; Riva, M.; Heikkinen, L.; Williams, J.; Fischer, H.; Lelieveld, J.; Crowley, J. N. Alkyl Nitrates in the Boreal Forest: Formation via the NO_3-, OH- and O_3-Induced Oxidation of Biogenic Volatile Organic Compounds and Ambient Lifetimes. *Atmos. Chem. Phys.* **2019**, *19* (15), 10391−10403.
(50) Gao, K.; Zhu, T. Analytical Methods for Organosulfate Detection in Aerosol Particles: Current Status and Future Perspectives. *Sci. Total Environ.* **2021**, *784*, 147244.
(51) Wang, Y.; Ren, J.; Huang, X. H. H.; Tong, R.; Yu, J. Z. Synthesis of Four Monoterpene-Derived Organosulfates and Their Quantification in Atmospheric Aerosol Samples. *Environ. Sci. Technol.* **2017**, *51* (12), 6791−6801.
(52) Huang, R.-J.; Cao, J.; Chen, Y.; Yang, L.; Shen, J.; You, Q.; Wang, K.; Lin, C.; Xu, W.; Gao, B.; Li, Y.; Chen, Q.; Hoffmann, T.; O'Dowd, C. D.; Bilde, M.; Glasius, M. Organosulfates in Atmospheric Aerosol: Synthesis and Quantitative Analysis of $PM_{2.5}$ from Xi'an, Northwestern China. *Atmos. Meas. Tech.* **2018**, *11* (6), 3447−3456.
(53) Hu, M.; Wang, Y.; Wang, S.; Jiao, M.; Huang, G.; Xia, B. Spatial-Temporal Heterogeneity of Air Pollution and Its Relationship with Meteorological Factors in the Pearl River Delta, China. *Atmos. Environ.* **2021**, *254*, 118415.
(54) Javed, M.; Bashir, M.; Zaineb, S. Analysis of Daily and Seasonal Variation of Fine Particulate Matter (PM2.5) for Five Cities of China. *Environ. Dev. Sustain.* **2021**, *23*, 12095−12123.
(55) Zou, Y.; Deng, X. J.; Deng, T.; Yin, C. Q.; Li, F. One-Year Characterization and Reactivity of Isoprene and Its Impact on Surface Ozone Formation at a Suburban Site in Guangzhou, China. *Atmosphere* **2019**, *10* (4), 201.

https://doi.org/10.1021/acsearthspacechem.1c00204
ACS Earth Space Chem. XXXX, XXX, XXX−XXX

(56) Surratt, J. D.; Gómez-González, Y.; Chan, A. W. H.; Vermeylen, R.; Shahgholi, M.; Kleindienst, T. E.; Edney, E. O.; Offenberg, J. H.; Lewandowski, M.; Jaoui, M.; Maenhaut, W.; Claeys, M.; Flagan, R. C.; Seinfeld, J. H. Organosulfate Formation in Biogenic Secondary Organic Aerosol. *J. Phys. Chem. A* **2008**, *112* (36), 8345−8378.
(57) Riva, M.; Budisulistiorini, S. H.; Zhang, Z.; Gold, A.; Surratt, J. D. Chemical Characterization of Secondary Organic Aerosol Constituents from Isoprene Ozonolysis in the Presence of Acidic Aerosol. *Atmos. Environ.* **2016**, *130*, 5−13.
(58) Nestorowicz, K.; Jaoui, M.; Rudzinski, K. J.; Lewandowski, M.; Kleindienst, T. E.; Spólnik, G.; Danikiewicz, W.; Szmigielski, R. Chemical Composition of Isoprene SOA under Acidic and Non-Acidic Conditions: Effect of Relative Humidity. *Atmos. Chem. Phys.* **2018**, *18* (24), 18101−18121.
(59) Cui, T.; Zeng, Z.; dos Santos, E. O.; Zhang, Z.; Chen, Y.; Zhang, Y.; Rose, C. A.; Budisulistiorini, S. H.; Collins, L. B.; Bodnar, W. M.; de Souza, R. A. F.; Martin, S. T.; Machado, C. M. D.; Turpin, B. J.; Gold, A.; Ault, A. P.; Surratt, J. D. Development of a Hydrophilic Interaction Liquid Chromatography (HILIC) Method for the Chemical Characterization of Water-Soluble Isoprene Epoxydiol (IEPOX)-Derived Secondary Organic Aerosol. *Environ. Sci. Process. Impacts* **2018**, *20* (11), 1524−1536.
(60) Trufelli, H.; Palma, P.; Famiglini, G.; Cappiello, A. An Overview of Matrix Effects in Liquid Chromatography-Mass Spectrometry. *Mass Spectrom. Rev.* **2011**, *30* (3), 491−509.
(61) Wang, Y.; Tong, R.; Yu, J. Z. Chemical Synthesis of Multifunctional Air Pollutants: Terpene-Derived Nitrooxy Organosulfates. *Environ. Sci. Technol.* **2021**, *55*, 8573.
(62) Xu, J.; Song, S.; Harrison, R. M.; Song, C.; Wei, L.; Zhang, Q.; Sun, Y.; Lei, L.; Zhang, C.; Yao, X.; Chen, D.; Li, W.; Wu, M.; Tian, H.; Luo, L.; Tong, S.; Li, W.; Wang, J.; Shi, G.; Huangfu, Y.; Tian, Y.; Ge, B.; Su, S.; Peng, C.; Chen, Y.; Yang, F.; Mihajlidi-Zelić, A.; Đordević, D.; Swift, S. J.; Andrews, I.; Hamilton, J. F.; Sun, Y.; Kramawijaya, A.; Han, J.; Saksakulkrai, S.; Baldo, C.; Hou, S.; Zheng, F.; Daellenbach, K. R.; Yan, C.; Liu, Y.; Kulmala, M.; Fu, P.; Shi, Z. An Interlaboratory Comparison of Aerosol Inorganic Ion Measurements by Ion Chromatography: Implications for Aerosol PH Estimate. *Atmos. Meas. Tech.* **2020**, *13* (11), 6325−6341.
(63) Newland, M. J.; Bryant, D. J.; Dunmore, R. E.; Bannan, T. J.; Joe, W.; Langford, B.; Hopkins, J. R.; Squires, F. A.; Dixon, W.; Drysdale, W. S.; Ivatt, P. D.; Evans, M. J.; Edwards, P. M.; Whalley, L. K.; Heard, D. E.; Slater, E. J.; Woodward-Massey, R.; Ye, C.; Mehra, A.; Worrall, S. D.; Bacak, A.; Coe, H.; Percival, C. J.; Nicholas Hewitt, C.; Lee, J. D.; Cui, T.; Surratt, J. D.; Wang, X.; Lewis, A. C.; Rickard, A. R.; Hamilton, J. F. Low-NO Atmospheric Oxidation Pathways in a Polluted Megacity. *Atmos. Chem. Phys.* **2021**, *21* (3), 1613−1625.
(64) Sheehan, P. E.; Bowman, F. M. Estimated Effects of Temperature on Secondary Organic Aerosol Concentrations. *Environ. Sci. Technol.* **2001**, *35* (11), 2129−2135.
(65) Zheng, J.; Zheng, Z.; Yu, Y.; Zhong, L. Temporal, Spatial Characteristics and Uncertainty of Biogenic VOC Emissions in the Pearl River Delta Region, China. *Atmos. Environ.* **2010**, *44* (16), 1960−1969.
(66) Hatch, L. E.; Jen, C. N.; Kreisberg, N. M.; Selimovic, V.; Yokelson, R. J.; Stamatis, C.; York, R. A.; Foster, D.; Stephens, S. L.; Goldstein, A. H.; Barsanti, K. C. Highly Speciated Measurements of Terpenoids Emitted from Laboratory and Mixed-Conifer Forest Prescribed Fires. *Environ. Sci. Technol.* **2019**, *53* (16), 9418−9428.
(67) Ciccioli, P.; Brancaleoni, E.; Frattoni, M.; Cecinato, A.; Pinciarelli, L. Determination of Volatile Organic Compounds (VOC) Emitted from Biomass Burning of Mediterranean Vegetation Species by GC-MS. *Anal. Lett.* **2006**, *34* (6), 937−955.
(68) Gilman, J. B.; Lerner, B. M.; Kuster, W. C.; Goldan, P. D.; Warneke, C.; Veres, P. R.; Roberts, J. M.; De Gouw, J. A.; Burling, I. R.; Yokelson, R. J. Biomass Burning Emissions and Potential Air Quality Impacts of Volatile Organic Compounds and Other Trace Gases from Fuels Common in the US. *Atmos. Chem. Phys.* **2015**, *15* (24), 13915−13938.
(69) McDonald, J. D.; Zielinska, B.; Fujita, E. M.; Sagebiel, J. C.; Chow, J. C.; Watson, J. G. Fine Particle and Gaseous Emission Rates from Residential Wood Combustion. *Environ. Sci. Technol.* **2000**, *34* (11), 2080−2091.
(70) Hatch, L. E.; Luo, W.; Pankow, J. F.; Yokelson, R. J.; Stockwell, C. E.; Barsanti, K. C. Identification and Quantification of Gaseous Organic Compounds Emitted from Biomass Burning Using Two-Dimensional Gas Chromatography-Time-of-Flight Mass Spectrometry. *Atmos. Chem. Phys.* **2015**, *15* (4), 1865−1899.
(71) Stewart, G. J.; Acton, W. J. F.; Nelson, B. S.; Vaughan, A. R.; Hopkins, J. R.; Arya, R.; Mondal, A.; Jangirh, R.; Ahlawat, S.; Yadav, L.; Sharma, S. K.; Dunmore, R. E.; Yunus, S. S. M.; Hewitt, C. N.; Nemitz, E.; Mullinger, N.; Gadi, R.; Sahu, L. K.; Tripathi, N.; Rickard, A. R.; Lee, J. D.; Mandal, T. K.; Hamilton, J. F. Emissions of Non-Methane Volatile Organic Compounds from Combustion of Domestic Fuels in Delhi, India. *Atmos. Chem. Phys.* **2021**, *21* (4), 2383−2406.
(72) Klein, F.; Farren, N. J.; Bozzetti, C.; Daellenbach, K. R.; Kilic, D.; Kumar, N. K.; Pieber, S. M.; Slowik, J. G.; Tuthill, R. N.; Hamilton, J. F.; Baltensperger, U.; Prévôt, A. S. H.; El Haddad, I. Indoor Terpene Emissions from Cooking with Herbs and Pepper and Their Secondary Organic Aerosol Production Potential. *Sci. Rep.* **2016**, *6* (1), 1−7.
(73) Wang, Y.; Hu, M.; Guo, S.; Wang, Y.; Zheng, J.; Yang, Y.; Zhu, W.; Tang, R.; Li, X.; Liu, Y.; Le Breton, M.; Du, Z.; Shang, D.; Wu, Y.; Wu, Z.; Song, Y.; Lou, S.; Hallquist, M.; Yu, J. The Secondary Formation of Organosulfates under Interactions between Biogenic Emissions and Anthropogenic Pollutants in Summer in Beijing. *Atmos. Chem. Phys.* **2018**, *18* (14), 10693−10713.
(74) He, Q.-F.; Ding, X.; Wang, X.-M.; Yu, J.-Z.; Fu, X.-X.; Liu, T.-Y.; Zhang, Z.; Xue, J.; Chen, D.-H.; Zhong, L.-J.; Donahue, N. M. Organosulfates from Pinene and Isoprene over the Pearl River Delta, South China: Seasonal Variation and Implication in Formation Mechanisms. *Environ. Sci. Technol.* **2014**, *48* (16), 9236−9245.
(75) Xu, L.; Yang, Z.; Tsona, N. T.; Wang, X.; George, C.; Du, L. Anthropogenic−Biogenic Interactions at Night: Enhanced Formation of Secondary Aerosols and Particulate Nitrogen- and Sulfur-Containing Organics from β-Pinene Oxidation. *Environ. Sci. Technol.* **2021**, *55*, 7794.
(76) Ye, C.; Yuan, B.; Lin, Y.; Wang, Z.; Hu, W.; Li, T.; Chen, W.; Wu, C.; Wang, C.; Huang, S.; Qi, J.; Wang, B.; Wang, C.; Song, W.; Wang, X.; Zheng, E.; Krechmer, J. E.; Ye, P.; Zhang, Z.; Wang, X.; Worsnop, D. R.; Shao, M. Chemical Characterization of Oxygenated Organic Compounds in the Gas Phase and Particle Phase Using Iodide CIMS with FIGAERO in Urban Air. *Atmos. Chem. Phys.* **2021**, *21* (11), 8455−8478.
(77) Suarez-Bertoa, R.; Picquet-Varrault, B.; Tamas, W.; Pangui, E.; Doussin, J. F. Atmospheric Fate of a Series of Carbonyl Nitrates: Photolysis Frequencies and OH-Oxidation Rate Constants. *Environ. Sci. Technol.* **2012**, *46* (22), 12502−12509.
(78) Photolytically Induced Changes in Composition and Volatility of Biogenic Secondary Organic Aerosol from Nitrate Radical Oxidation during Night-to-day Transition. https://acp.copernicus.org/preprints/acp-2021-347/ (accessed 2021-05-16).
(79) Atkinson, R. Gas-Phase Tropospheric Chemistry of Volatile Organic Compounds: 1. Alkanes and Alkenes. *J. Phys. Chem. Ref. Data* **1997**, *26* (2), 215−290.
(80) Jones, C. E.; Hopkins, J. R.; Lewis, A. C. In Situ Measurements of Isoprene and Monoterpenes within a South-East Asian Tropical Rainforest. *Atmos. Chem. Phys.* **2011**, *11* (14), 6971−6984.
(81) Drozd, G. T.; Woo, J. L.; McNeill, V. F. Self-Limited Uptake of α-Pinene Oxide to Acidic Aerosol: The Effects of Liquid-Liquid Phase Separation and Implications for the Formation of Secondary Organic Aerosol and Organosulfates from Epoxides. *Atmos. Chem. Phys.* **2013**, *13* (16), 8255−8263.
(82) Kwan, A. J.; Chan, A. W. H.; Ng, N. L.; Kjaergaard, H. G.; Seinfeld, J. H.; Wennberg, P. O. Peroxy Radical Chemistry and OH Radical Production during the NO_3 -Initiated Oxidation of Isoprene. *Atmos. Chem. Phys.* **2012**, *12* (16), 7499−7515.

https://doi.org/10.1021/acsearthspacechem.1c00204
ACS Earth Space Chem. XXXX, XXX, XXX−XXX

(83) Schwantes, R. H.; Charan, S. M.; Bates, K. H.; Huang, Y.; Nguyen, T. B.; Mai, H.; Kong, W.; Flagan, R. C.; Seinfeld, J. H. Low-Volatility Compounds Contribute Significantly to Isoprene Secondary Organic Aerosol (SOA) under High-NO_X Conditions. *Atmos. Chem. Phys.* **2019**, *19* (11), 7255−7278.
(84) Rattanavaraha, W.; Chu, K.; Budisulistiorini, S. H.; Riva, M.; Lin, Y.-H.; Edgerton, E. S.; Baumann, K.; Shaw, S. L.; Guo, H.; King, L.; Weber, R. J.; Neff, M. E.; Stone, E. A.; Offenberg, J. H.; Zhang, Z.; Gold, A.; Surratt, J. D. Assessing the Impact of Anthropogenic Pollution on Isoprene-Derived Secondary Organic Aerosol Formation in $PM_{2.5}$ Collected from the Birmingham, Alabama, Ground Site during the 2013 Southern Oxidant and Aerosol Study. *Atmos. Chem. Phys.* **2016**, *16* (8), 4897−4914.
(85) Kourtchev, I.; Godoi, R. H. M.; Connors, S.; Levine, J. G.; Archibald, A. T.; Godoi, A. F. L.; Paralovo, S. L.; Barbosa, C. G. G.; Souza, R. A. F.; Manzi, A. O.; Seco, R.; Sjostedt, S.; Park, J. H.; Guenther, A.; Kim, S.; Smith, J.; Martin, S. T.; Kalberer, M. Molecular Composition of Organic Aerosols in Central Amazonia: An Ultra-High-Resolution Mass Spectrometry Study. *Atmos. Chem. Phys.* **2016**, *16* (18), 11899−11913.
(86) Lin, Y. H.; Zhang, Z.; Docherty, K. S.; Zhang, H.; Budisulistiorini, S. H.; Rubitschun, C. L.; Shaw, S. L.; Knipping, E. M.; Edgerton, E. S.; Kleindienst, T. E.; Gold, A.; Surratt, J. D. Isoprene Epoxydiols as Precursors to Secondary Organic Aerosol Formation: Acid-Catalyzed Reactive Uptake Studies with Authentic Compounds. *Environ. Sci. Technol.* **2012**, *46* (1), 250−258.
(87) Nguyen, T. B.; Coggon, M. M.; Bates, K. H.; Zhang, X.; Schwantes, R. H.; Schilling, K. A.; Loza, C. L.; Flagan, R. C.; Wennberg, P. O.; Seinfeld, J. H. Organic Aerosol Formation from the Reactive Uptake of Isoprene Epoxydiols (IEPOX) onto Non-Acidified Inorganic Seeds. *Atmos. Chem. Phys.* **2014**, *14* (7), 3497−3510.
(88) Worton, D. R.; Surratt, J. D.; Lafranchi, B. W.; Chan, A. W. H.; Zhao, Y.; Weber, R. J.; Park, J. H.; Gilman, J. B.; De Gouw, J.; Park, C.; Schade, G.; Beaver, M.; Clair, J. M. S.; Crounse, J.; Wennberg, P.; Wolfe, G. M.; Harrold, S.; Thornton, J. A.; Farmer, D. K.; Docherty, K. S.; Cubison, M. J.; Jimenez, J. L.; Frossard, A. A.; Russell, L. M.; Kristensen, K.; Glasius, M.; Mao, J.; Ren, X.; Brune, W.; Browne, E. C.; Pusede, S. E.; Cohen, R. C.; Seinfeld, J. H.; Goldstein, A. H. Observational Insights into Aerosol Formation from Isoprene. *Environ. Sci. Technol.* **2013**, *47* (20), 11403−11413.
(89) Lee, J. D.; Lewis, A. C.; Monks, P. S.; Jacob, M.; Hamilton, J. F.; Hopkins, J. R.; Watson, N. M.; Saxton, J. E.; Ennis, C.; Carpenter, L. J.; Carslaw, N.; Fleming, Z.; Bandy, B. J.; Oram, D. E.; Penkett, S. A.; Slemr, J.; Norton, E.; Rickard, A. R.; K Whalley, L.; Heard, D. E.; Bloss, W. J.; Gravestock, T.; Smith, S. C.; Stanton, J.; Pilling, M. J.; Jenkin, M. E. Ozone Photochemistry and Elevated Isoprene during the UK Heatwave of August 2003. *Atmos. Environ.* **2006**, *40* (39), 7598−7613.

https://doi.org/10.1021/acsearthspacechem.1c00204
ACS Earth Space Chem. XXXX, XXX, XXX−XXX